



UV–OPTICAL OBSERVATION OF TYPE Ia SUPERNOVA SN 2013dy IN NGC 7250

QIAN ZHAI^{1,2,3}, JU-JIA ZHANG^{1,3}, XIAO-FENG WANG⁴, TIAN-MENG ZHANG⁵, ZHENG-WEI LIU⁶, PETER J. BROWN⁷, FAN HUANG⁴, XU-LIN ZHAO⁴, LIANG CHANG^{1,3}, WEI-MIN YI^{1,3}, CHUAN-JUN WANG^{1,3}, YU-XIN XIN^{1,3}, JIAN-GUO WANG^{1,3}, BAO-LI LUN^{1,3}, XI-LIANG ZHANG^{1,3}, YU-FENG FAN^{1,3}, XIANG-MING ZHENG^{1,3}, AND JIN-MING BAI^{1,3}

¹ Yunnan Observatories (YNAO), Chinese Academy of Sciences, Kunming 650011, China; jujia@ynao.ac.cn

² University of Chinese Academy of Sciences, Chinese Academy of Sciences, Beijing 100049, China

³ Key Laboratory for the Structure and Evolution of Celestial Objects, Chinese Academy of Sciences, Kunming 650011, China

⁴ Physics Department and Tsinghua Center for Astrophysics (THCA), Tsinghua University, Beijing 100084, China

⁵ National Astronomical Observatories of China (NAOC), Chinese Academy of Sciences, Beijing 100012, China

⁶ Argelander-Institut für Astronomie, Auf dem Hügel 71, D-53121, Bonn, Germany

⁷ George P. and Cynthia Woods Mitchell Institute for Fundamental Physics & Astronomy, Texas A. & M. University, Department of Physics and Astronomy, 4242 TAMU, College Station, TX 77843, USA

Received 2015 August 8; accepted 2016 February 16; published 2016 April 26

ABSTRACT

Extensive and independent observations of Type Ia supernova (SN Ia) SN 2013dy are presented, including a larger set of *UBVRI* photometry and optical spectra from a few days before the peak brightness to ~ 200 days after explosion, and ultraviolet (UV) photometry spanning from $t \approx -10$ days to $t \approx +15$ days refers to the *B* band maximum. The peak brightness (i.e., $M_B = -19.65 \pm 0.40$ mag; $L_{\max} = [1.95 \pm 0.55] \times 10^{43}$ erg s⁻¹) and the mass of synthesized ⁵⁶Ni (i.e., $M(^{56}\text{Ni}) = 0.90 \pm 0.26 M_{\odot}$) are calculated, and they conform to the expectation for an SN Ia with a slow decline rate (i.e., $\Delta m_{15}(B) = 0.90 \pm 0.03$ mag). However, the near infrared (NIR) brightness of this SN (i.e., $M_H = -17.33 \pm 0.30$ mag) is at least 1.0 mag fainter than usual. Besides, spectroscopy classification reveals that SN 2013dy resides on the border of “core normal” and “shallow silicon” subclasses in the Branch et al. classification scheme, or on the border of the “normal velocity” SNe Ia and 91T/99aa-like events in the Wang et al. system. These suggest that SN 2013dy is a slow-declining SN Ia located on the transitional region of nominal spectroscopic subclasses and might not be a typical normal sample of SNe Ia.

Key words: galaxies: individual (NGC 7250) – supernovae: general – supernovae: individual (SN 2013dy)

1. INTRODUCTION

SN 2013dy, an SN Ia, was discovered at roughly a magnitude of ~ 17.2 mag on UT July 10.45 2013 (Universal Time is used throughout this paper) in an unfiltered image of the galaxy NGC 7250 by the Lick observatory supernova search (Casper et al. 2013). Its coordinates are R. A. = 22^h 18^m 17^s.60, decl. = +40° 34' 9".54 (J2000) and it is located at 2"3 west and 26"4 north of the center of the host galaxy (see Figure 1). It was well studied by Zheng et al. (2013, hereafter Z13) at early phase, based on the dense photometries ($t \approx -17$ to +3 days; the variable t denotes the time since *B* band maximum and is used throughout this paper) and spectra ($t \approx -16$ to -6 days). Pan et al. (2015, hereafter P15) also investigated this SN from the *BVRiLiZYJH* band photometry and UV–optical spectroscopy data set spanning from ~ 0.1 to ~ 500 days after explosion.

Based on the discovery and pre-discovery images, Z13 constrained the first-light time (i.e., JD 2456483.18) of SN 2013dy to be only 2.4 ± 1.2 hr before the first detection. This makes it the earliest known detection of an SN Ia. They inferred an upper limit on the radius of the progenitor star of $R_0 \leq 0.25 R_{\odot}$ through the early-time observations, which is consistent with that of a white dwarf progenitor. The early rising light curve exhibits a broken power law with exponents of 0.88 and then 1.80, which suggests that the rising exponent of SNe Ia may vary with time. Besides, Z13 derived that SN 2013dy reached a *B* band maximum at ~ 17.7 days after first light with $m(B)_{\max} = 13.28 \pm 0.01$ mag. A spectrum taken at $t \approx -16$ days reveals a C II $\lambda 6580$ absorption line comparable in strength to Si II $\lambda 6355$. Such strong C II lines are not usually seen in normal SNe Ia, but similar features have been observed

in a few superluminous SNe Ia (i.e., SN 2009dc; Taubenberger et al. 2010). This feature suggests that the progenitor star had significant unburned material.

In this paper, we present extensive and independent UV–optical photometry and optical spectroscopy of SN 2013dy. Additionally, the *BVRI* photometry of Z13 and the *BVRIYJH* photometry of P15 are also involved in the analysis. Note that the UV and *U* band photometry in this paper are unique and important for further investigation since these data are not involved in Z13 and P15. On the other hand, our dense *BVRI* photometry and low-resolution spectra can fill the observational gaps in Z13 and P15 in the first 200 days after explosion, which makes SN 2013dy a super well-sampled SN Ia. That could provide highly constraining information in investigating the properties of SNe Ia. Furthermore, the large data set presented in this paper can help us further understand the diversity of SNe Ia and their impact on cosmological applications.

The organization of this paper is as follows. Observations and data reductions are described in Section 2. Section 3 investigates the light and color curves, and estimates the extinction owing to the host galaxy. Section 4 presents the spectra evolution. In Section 5, we estimate the distance of this SN, construct the spectral energy distribution (SED) and bolometric light curve, estimate the mass of synthesized ⁵⁶Ni, and discuss the spectroscopic classification. A brief summary is given in Section 6.

2. OBSERVATIONS AND DATA REDUCTIONS

NGC 7250, the host galaxy of SN 2013dy, is an irregular galaxy characterized by the “dual cores” in the center; see

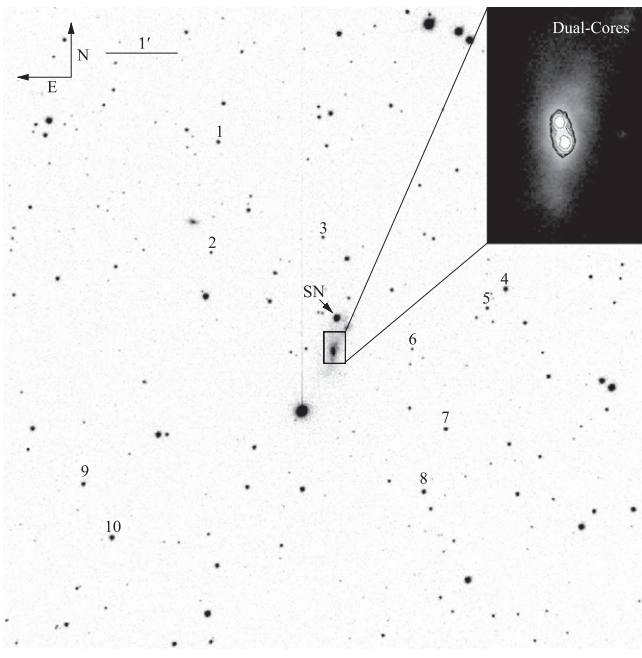


Figure 1. *R* band image of SN 2013dy and its reference stars, taken with the LJT and YFOSC on 2013 July 27.73. The mean FWHM of this image is $\sim 1''.10$ under the scale of $\sim 0''.283/\text{pix}$.

the top right panel of Figure 1. These two cores at a distance of $\sim 2''.38$ or ~ 230 pc refer to the distance of NGC 7250 derived in this paper (i.e., $D = 20.0 \pm 4.0$ Mpc). The dual-core feature might be interpreted by the interaction of two galaxies in the past. Z13 also noted that there is a bright, blue region at $\sim 8''.7$ west and $\sim 6''.4$ south of this SN (projected distance $D = \sim 1.2$ kpc), which might relate to the merging history.

Our first observation of this supernova is in spectroscopy on 2013 July 14 (Zhang & Wang 2013; 4.76 days after the first light and published in Z13) with the Yunnan Faint Object Spectrograph and Camera (YFOSC; Zhang et al. 2014) mounted at the Li-Jiang 2.4 m telescope (hereafter LJT; Fan et al. 2015) of Yunnan Observatories (YNAO), China. About two weeks later, we started to monitor this transient intensively at LJT in both photometry and spectroscopy spanning from $t \approx +0$ to $t \approx +180$ days. Optical photometry data are also collected with the Tsinghua-NAOC 0.8 m telescope (hereafter TNT; Wang et al. 2008; Huang et al. 2012) at Xing-Long Observation of National Astronomical Observatories (NAOC), China, from $t \approx -2$ days to $t \approx +150$ days. Additionally, three spectra were obtained at the Xing-Long 2.16 m telescope (hereafter XLT) with the Bei-Jing Faint Object Spectrograph and Camera (BFOSC). Furthermore, this target was also observed by the UVOT (Romig et al. 2005) on board the *Swift* satellite (Gehrels et al. 2004), spanning from $t \approx -10$ days to $t \approx +15$ days in the UV and optical bands.

2.1. Photometry

2.1.1. Ground-based Observation

The ground-based optical photometry of SN 2013dy were obtained in the *UBVRI* bands with the LJT and TNT, covering the period from $t \approx -2$ days to $t \approx +180$ days. All of the CCD

Table 1
Photometric Standards in the Field of SN 2013dy

Star	<i>U</i> (mag)	<i>B</i> (mag)	<i>V</i> (mag)	<i>R</i> (mag)	<i>I</i> (mag)
1	16.49(02)	16.32(02)	15.61(02)	15.29(01)	14.93(01)
2	17.61(04)	17.27(03)	16.57(01)	16.12(01)	15.78(01)
3	17.26(03)	17.09(03)	16.47(02)	16.05(01)	15.73(01)
4	16.52(02)	15.92(01)	15.09(01)	14.59(01)	14.22(01)
5	16.79(02)	16.72(01)	16.16(01)	15.78(01)	15.48(01)
6	18.18(02)	17.81(02)	17.05(03)	16.65(02)	16.26(01)
7	16.31(02)	16.27(03)	15.68(01)	15.34(01)	15.03(02)
8	15.77(02)	15.73(01)	15.18(01)	14.87(01)	14.56(01)
9	16.34(02)	16.20(01)	15.58(01)	15.22(01)	14.90(01)
10	16.36(03)	15.79(03)	14.97(01)	14.52(02)	14.18(01)

Note. Uncertainties, in units of 0.01 mag, are 1σ . See Figure 1 for the finding chart of SN 2013dy and the reference stars.

images are reduced using the IRAF⁸ standard procedure, including the corrections for bias, overscan, flat field, and removal of cosmic rays. There were a few groups of templates obtained at LJT and TNT in the winter of 2014 when the SN vanished. These templates are applied to the host subtraction of the corresponding data. Based on the subtracted images, we measured the instrumental magnitude of this SN through the aperture photometry of the IRAF DAOPHOT package (Stetson 1987). Ten local standard stars in the field of SN 2013dy are labeled in Figure 1. These reference stars are converted to the standard Johnson *UBV* (Johnson et al. 1966) and Kron-Cousins *RI* (Cousins 1981) systems through transformations established by observing Landolt (1992) standard stars during several photometric nights. The magnitudes of these stars, as listed in Table 1, are then applied to transform the instrumental magnitudes of SN 2013dy to the standard *UBVRI* system, as listed in Table 2.

2.1.2. Space-based Observation

The *Swift* observatory (Gehrels et al. 2004) began observing SN 2013dy on 2013 July 17.09, about 10 days before the *B* band maximum, and continued for approximately 26 days. These photometric observations are performed in three UV filters (*uvw2*, *uvm2*, and *uvw1*) and three broadband optical filters (*uu*, *bb*, and *vv*). The photometry presented here are reduced using the *Swift* Optical/Ultraviolet Supernova Archive (SOUSA; Brown et al. 2014) reductions, including subtraction of the underlying host galaxy flux using *Swift*-UVOT observations from 2014 March and April. Table 3 lists the final UVOT UV/optical magnitudes of SN 2013dy. The results of *uvw2* and *uvw1* are also corrected for the “red tail” (Brown et al. 2010) of each filter. The color-term corrections (Poole et al. 2008) have been further applied to the magnitudes of the UVOT optical filters of the standard Johnson *UBV* bands when these data are plotted in the Figure 2.

2.2. Spectroscopy

A journal of the spectroscopic observation of SN 2013dy is given in Table 4, containing 21 low-resolution spectra spanning from $t \approx +0$ to $+180$ days; see also Figure 3. All spectra were

⁸ IRAF, the Image Reduction and Analysis Facility, is distributed by the National Optical Astronomy Observatory, which is operated by the Association of Universities for Research in Astronomy (AURA), Inc. under cooperative agreement with the National Science Foundation (NSF).

Table 2
The *UBVRI* Photometry of SN 2013dy from the Ground-based Observations

MJD	Day ^a	<i>U</i> (mag)	<i>B</i> (mag)	<i>V</i> (mag)	<i>R</i> (mag)	<i>I</i> (mag)	Telescope
56498.11	-2.77	12.87(03)	13.38(01)	13.08(01)	12.96(01)	12.98(01)	TNT
56499.12	-1.76	12.88(02)	13.36(01)	13.04(01)	12.93(01)	13.00(01)	TNT
56500.72	-0.16	12.89(03)	13.28(01)	12.96(01)	12.85(01)	12.96(01)	LJT
56502.09	1.21	12.94(02)	13.28(01)	12.94(01)	12.82(01)	12.98(01)	TNT
56504.70	3.82	13.09(03)	13.36(01)	12.99(01)	12.87(01)	13.09(01)	LJT
56506.63	5.75	13.28(03)	13.44(01)	13.03(01)	12.93(01)	13.17(01)	LJT
56507.62	6.74	13.42(04)	13.52(01)	13.05(01)	12.97(01)	13.21(01)	LJT
56511.65	10.77	13.89(02)	13.82(02)	13.22(02)	13.15(02)	13.37(03)	LJT
56513.76	12.88	14.12(02)	14.01(02)	13.34(02)	13.26(03)	13.45(02)	LJT
56516.76	15.88	14.43(04)	14.29(03)	13.52(03)	13.38(02)	13.54(03)	LJT
56517.76	16.88	14.52(04)	14.38(01)	13.55(01)	13.42(01)	13.59(01)	LJT
56519.75	18.87	14.75(02)	14.52(01)	13.65(01)	13.51(01)	13.64(01)	LJT
56521.71	20.83	14.97(02)	14.73(01)	13.76(01)	13.59(01)	13.61(01)	LJT
56523.34	22.46	...	14.83(01)	13.85(01)	13.64(01)	13.57(01)	TNT
56526.04	25.16	15.44(06)	15.08(01)	13.94(01)	13.67(01)	13.51(01)	TNT
56526.78	25.90	15.38(02)	15.18(01)	13.97(01)	13.68(01)	13.49(01)	LJT
56527.74	26.86	15.47(02)	15.23(01)	14.03(01)	13.69(01)	13.46(01)	LJT
56528.03	27.15	15.53(04)	15.23(01)	14.05(01)	13.69(01)	13.48(01)	TNT
56529.05	28.17	15.60(03)	15.31(01)	14.10(01)	13.73(01)	13.45(01)	TNT
56530.03	29.15	15.71(05)	15.40(02)	14.14(01)	13.73(01)	13.44(01)	TNT
56532.49	31.61	15.84(04)	15.56(03)	14.28(02)	13.81(02)	13.43(03)	LJT
56535.21	34.33	16.01(03)	15.76(01)	14.42(01)	13.94(01)	13.49(01)	TNT
56537.50	36.62	16.05(02)	15.90(01)	14.55(01)	14.05(01)	13.58(01)	LJT
56540.51	39.63	16.23(04)	16.04(02)	14.68(03)	14.23(03)	13.74(02)	LJT
56545.50	44.62	16.45(03)	16.20(02)	14.89(02)	14.50(02)	14.09(03)	LJT
56546.34	45.46	...	16.14(02)	14.93(01)	14.55(01)	14.14(01)	TNT
56547.34	46.46	...	16.21(03)	14.97(01)	14.61(01)	14.23(01)	TNT
56550.32	49.44	...	16.24(02)	15.05(01)	14.68(01)	14.37(01)	TNT
56554.52	53.64	16.68(04)	16.35(03)	15.18(03)	14.88(02)	14.55(02)	LJT
56560.32	59.44	...	16.41(02)	15.33(01)	15.03(01)	14.81(01)	TNT
56561.31	60.43	...	16.43(02)	15.37(01)	15.06(01)	14.88(01)	TNT
56562.30	61.42	...	16.41(02)	15.38(01)	15.10(01)	14.93(01)	TNT
56563.30	62.42	...	16.51(04)	15.41(02)	15.19(01)	14.95(01)	TNT
56564.50	63.62	16.94(03)	16.44(01)	15.47(01)	15.18(01)	15.01(01)	LJT
56565.50	64.62	16.98(03)	16.54(01)	15.48(01)	15.21(01)	15.08(01)	LJT
56574.05	73.17	17.21(13)	16.56(03)	15.69(02)	15.49(02)	15.41(02)	TNT
56574.53	73.65	17.21(03)	16.62(01)	15.67(01)	15.46(01)	15.41(01)	LJT
56575.52	74.64	17.24(03)	16.65(01)	15.71(01)	15.49(01)	15.46(01)	LJT
56576.10	75.22	...	16.58(02)	15.73(01)	15.49(01)	15.46(01)	TNT
56576.52	75.64	17.27(03)	16.67(01)	15.74(01)	15.52(01)	15.50(01)	LJT
56576.96	76.08	...	16.66(02)	15.80(01)	15.56(01)	15.55(01)	TNT
56579.97	79.09	...	16.73(02)	15.83(01)	15.62(01)	15.67(01)	TNT
56583.52	82.64	17.43(03)	16.80(01)	15.93(01)	15.71(01)	15.77(01)	LJT
56584.96	84.08	...	16.68(03)	16.00(02)	15.76(02)	15.82(02)	TNT
56585.98	85.10	...	16.72(03)	15.96(02)	15.83(01)	15.86(02)	TNT
56586.97	86.09	17.48(13)	16.84(03)	16.01(02)	15.87(02)	15.90(02)	TNT
56588.95	88.07	...	16.82(02)	16.08(01)	15.90(01)	16.02(01)	TNT
56589.52	88.64	17.58(03)	16.86(01)	16.08(01)	15.91(01)	15.99(01)	LJT
56589.98	89.10	...	16.85(02)	16.11(01)	15.96(01)	16.06(01)	TNT
56594.52	93.64	17.73(03)	16.92(01)	16.21(01)	16.08(01)	16.17(01)	LJT
56595.18	94.30	17.76(03)	16.95(01)	16.25(01)	16.11(01)	16.20(01)	LJT
56596.18	95.30	17.82(03)	16.99(01)	16.28(01)	16.14(01)	16.23(01)	LJT
56601.96	101.08	...	17.03(02)	16.39(01)	16.33(01)	16.46(01)	TNT
56602.99	102.11	...	17.07(02)	16.41(01)	16.33(01)	16.50(01)	TNT
56603.98	103.10	...	17.07(02)	16.40(01)	16.34(01)	16.46(01)	TNT
56606.96	106.08	...	17.12(02)	16.38(01)	16.37(01)	16.51(01)	TNT
56608.00	107.12	...	17.16(02)	16.52(01)	16.47(01)	16.68(01)	TNT
56608.99	108.11	...	17.15(02)	16.52(01)	16.52(01)	16.72(02)	TNT
56610.49	109.61	18.01(03)	17.19(01)	16.52(01)	16.57(01)	16.65(01)	LJT
56610.99	110.11	...	17.18(02)	16.51(01)	16.49(01)	16.74(01)	TNT
56612.01	111.13	...	17.25(02)	16.69(02)	16.59(02)	16.80(02)	TNT
56612.48	111.60	18.23(03)	17.23(01)	16.61(01)	16.62(01)	16.72(01)	LJT
56612.96	112.08	...	17.22(02)	16.57(02)	16.60(02)	16.81(02)	TNT
56614.01	113.13	...	17.19(03)	16.53(02)	16.47(02)	16.83(02)	TNT

Table 2
(Continued)

MJD	Day ^a	<i>U</i> (mag)	<i>B</i> (mag)	<i>V</i> (mag)	<i>R</i> (mag)	<i>I</i> (mag)	Telescope
56615.12	114.24	...	17.21(03)	16.67(02)	16.54(02)	16.84(02)	TNT
56615.98	115.10	18.26(13)	17.28(02)	16.67(02)	16.69(02)	16.86(02)	TNT
56616.98	116.10	...	17.27(03)	16.56(05)	16.74(01)	16.94(02)	TNT
56617.97	117.09	...	17.33(02)	16.74(01)	16.79(01)	16.96(02)	TNT
56618.98	118.10	...	17.33(02)	16.78(02)	16.80(01)	17.03(02)	TNT
56619.97	119.09	...	17.35(03)	16.80(02)	16.86(02)	17.08(02)	TNT
56620.98	120.10	...	17.29(02)	16.77(01)	16.87(01)	17.08(02)	TNT
56621.98	121.10	...	17.31(02)	16.80(01)	16.88(01)	17.09(02)	TNT
56628.47	127.59	...	17.45(01)	16.92(01)	17.06(01)	17.17(01)	LJT
56629.96	129.08	...	17.46(03)	16.97(02)	17.09(02)	17.36(02)	TNT
56630.49	129.61	18.48(05)	17.48(01)	17.00(01)	17.11(01)	17.20(01)	LJT
56631.95	131.07	...	17.50(02)	17.00(01)	17.15(01)	17.32(02)	TNT
56632.98	132.10	...	17.56(02)	17.08(01)	17.22(02)	17.39(02)	TNT
56633.96	133.08	16.97(02)	17.20(02)	17.48(02)	TNT
56635.96	135.08	...	17.52(02)	17.10(02)	17.24(01)	17.44(02)	TNT
56636.92	136.04	16.94(02)	17.17(02)	17.57(02)	TNT
56639.93	139.05	...	17.64(03)	17.21(02)	17.34(02)	17.55(02)	TNT
56641.95	141.07	...	17.62(03)	17.18(02)	17.42(02)	17.51(02)	TNT
56645.96	145.08	...	17.72(02)	17.20(02)	17.40(02)	...	TNT
56646.96	146.08	...	17.69(02)	17.18(02)	17.49(02)	...	TNT
56647.54	146.66	...	17.69(02)	17.22(02)	17.54(01)	17.67(04)	LJT
56647.96	147.08	...	17.77(03)	17.28(02)	17.61(03)	...	TNT
56648.95	148.07	...	17.76(03)	17.28(02)	17.48(02)	...	TNT
56649.95	149.07	...	17.78(03)	17.34(02)	17.65(03)	...	TNT
56652.49	151.61	19.02(08)	17.87(02)	17.39(01)	17.63(03)	17.76(03)	LJT
56661.53	160.65	...	17.98(02)	17.52(02)	17.76(02)	17.96(03)	LJT
56664.55	163.67	...	18.04(02)	17.61(02)	17.80(02)	17.97(04)	LJT
56666.49	165.61	19.28(08)	18.07(03)	17.64(01)	17.89(02)	17.99(04)	LJT
56671.49	170.61	...	18.14(02)	17.76(02)	18.01(02)	18.14(06)	LJT
56674.50	173.62	19.47(09)	18.15(02)	17.71(01)	18.13(03)	18.21(05)	LJT
56681.49	180.61	...	18.24(03)	17.77(01)	18.17(02)	18.31(05)	LJT
56683.49	182.61	...	18.27(04)	17.79(02)	18.23(03)	18.35(06)	LJT

Note. Uncertainties (numbers in brackets), in units of 0.01 mag, are 1σ ; MJD = JD−2400000.5.

^a Relative to the *B* band maximum, JD = 2456501.38.

reduced using standard IRAF long-slit spectra routines. The flux calibration was done with the standard spectrophotometric flux stars observed at a similar airmass on the same night and were double-checked with the synthetic photometry computed using Bessell (1990) passbands. The spectra were further corrected for the atmospheric absorption and telluric lines at each observatory.

3. LIGHT CURVES OF SN 2013DY

Figure 2 shows the optical and UV light curves of SN 2013dy, overplotted with that of two well-sampled normal SNe Ia: SN 2011fe and SN 2003du. The *BVRI* photometry of Z13 and *BVRIYJH* photometry of P15 are also exhibited. Note that the solid lines in this figure are based on the photometry of SN 2011fe: the UV curves are derived from the *Swift* photometry presented in Brown et al. (2012) and fitted with a low order polynomial; the optical curves are derived from the photometry presented in Zhang et al. (2016b); the near infrared (NIR) curves are based on the photometry presented in Matheson et al. (2012). The light curves of SN 2011fe in the UV and optical are stretched by a factor of 1.20 on the horizontal axis. On the other hand, the *J* and *H* band curves of SN 2011fe are stretched by a factor of 1.10. The dashed lines are based on the photometry of SN 2003du (Stanishev et al. 2007) with a stretch factor of 1.05. The *Y* band photometry of SN 2013dy (P15) is

also plotted in this figure and overplotted with a polynomial fit (dotted line). Detailed analyses are presented in the following sections.

3.1. Parameters of Photometry

Based on the photometry published in Z13, P15, and this paper, we derived the parameters of peak magnitudes, maximum dates, and light curve decline rates (i.e., Δm_{15}) through a low order polynomial fit, as listed in Table 5. It is found that SN 2013dy reaches a *B* band maximum brightness of 13.29 ± 0.01 mag on JD 2456501.38 ± 0.30 (2013 July 27.88), which is close to that in Z13 (i.e., $m_{\max}(B) = 13.28$ mag, JD = 2456500.88) and P15 (i.e., $m_{\max}(B) = 13.23$ mag, JD = 2456501.61). The observed *B* band decline rate is estimated as $\Delta m_{15}(B) = 0.90 \pm 0.03$ mag, which is close to the estimation in P15 (i.e., 0.92).

One can see that in Figure 2, the light curves of SN 2013dy resemble the stretched light curves of SN 2003du (i.e., $\Delta m_{15}(B) = 1.02$ mag; Stanishev et al. 2007) and SN 2011fe (i.e., $\Delta m_{15}(B) = 1.10$ mag; Munari et al. 2013), especially at $t < +20$ days. Note that the stretched curves of SN 2011fe decline with slower rates in the *VRI* bands but with a quicker rate in the *U* band than that of SN 2013dy and SN 2003du.

Table 3
Swift-UVOT Photometry of SN 2013dy

MJD	Day ^a	<i>uvw2</i>	<i>uvw2_{rc}</i> ^b	<i>uvm2</i>	<i>uvw1</i>	<i>uvw1_{rc}</i> ^b	<i>uu</i>	<i>bb</i>	<i>vv</i>
56490.12	-10.76	17.24(10)	19.31	18.89(23)	15.56(07)	15.83	13.80(04)	14.27(04)	14.04(05)
56492.61	-8.27	16.61(09)	18.39	18.10(14)	14.80(06)	14.96	13.13(03)	13.74(03)	13.58(04)
56492.61	-8.27	13.12(03)	13.72(03)	13.53(04)
56492.67	-8.21	13.09(03)	13.75(03)	13.41(04)
56492.67	-8.21	13.13(03)	13.66(03)	13.52(04)
56495.69	-5.19	14.46(06)	14.58	12.84(04)
56498.12	-2.76	16.17(08)	18.01	17.75(13)	14.42(05)	14.61	12.78(04)	13.28(04)	13.02(04)
56504.10	3.22	13.17(03)	13.28(03)	13.03(04)
56504.10	3.22	16.51(09)	19.60	17.74(10)	14.89(07)	15.50	13.07(03)	13.23(03)	12.95(03)
56504.16	3.28	13.12(03)	13.28(03)	13.04(04)
56504.16	3.28	13.05(03)	13.24(03)	13.00(03)
56507.50	6.62	13.44(04)	13.50(03)	13.09(04)
56507.50	6.62	13.50(03)	13.41(03)	13.08(03)
56507.77	6.89	16.81(10)	20.23	18.15(12)	15.32(07)	16.31	13.44(04)	13.44(03)	13.04(04)
56507.77	6.89	13.40(03)	13.38(03)	13.02(03)
56510.42	9.54	17.38(35)	22.51	...	15.47(07)	16.46	13.76(04)	13.59(03)	...
56510.42	9.54	13.72(04)	13.57(03)	...
56510.49	9.61	13.73(04)	13.44(03)	...
56510.49	9.61	13.74(04)	13.57(03)	...
56513.90	13.02	17.39(13)	21.47	18.78(18)	15.93(09)	17.47	14.18(05)	13.85(03)	13.43(04)
56513.90	13.02	14.16(04)	13.84(03)	13.31(04)
56516.10	15.22	14.54(06)	14.14(04)	13.54(04)
56516.10	15.22	17.56(14)	21.33	18.86(24)	16.27(09)	18.15	14.44(04)	14.10(03)	13.48(04)

Notes. Uncertainties (numbers in brackets), in units of 0.01 mag, are 1σ ; MJD = JD - 2400000.5.

^a Relative to the date of the *B* band maximum, JD = 2456501.38.

^b After “Red-tail” correction (Brown et al. 2010).

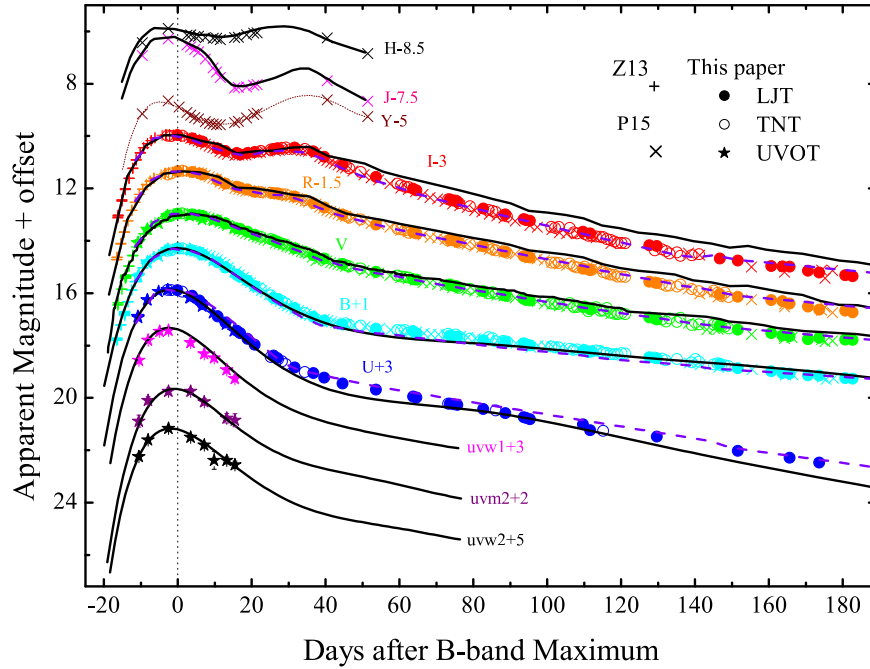


Figure 2. UV-optical-NIR light curves of SN 2013dy, which are shifted vertically for better display. The solid lines are derived from the photometry of SN 2011fe and the dashed lines from that of SN 2003du. The dotted line is for the interpolation of the *Y* band based on the photometry of SN 2013dy. See the text for detail.

3.2. Color Curves

Figure 4 shows the optical color curves of SN 2013dy, corrected for the Galactic reddening $E(B - V) = 0.15 \pm 0.02$ mag (Schlegel et al. 1998; Schlafly & Finkbeiner 2011) and the host galaxy reddening derived in Section 3.3. The Galactic reddening law (i.e., $R_V = 3.1$; Cardelli et al.

1989) is adopted for this correction. Overplotted are the color curves of SN 1999aa (Jha et al. 2006), SN 2003du (Stanishev et al. 2007), SN 2011fe (Zhang et al. 2016b), and SN 2012fr (Zhang et al. 2014). The overall color evolution of SN 2013dy is similar to that of SN 2003du, but distinctions are present in the colors of $U - B$ at the early phase. On the contrary, the

Table 4
Journal of Spectroscopic Observations of SN 2013dy

Date (UT)	MJD (−240000.5)	Epoch ^a (days)	Res. (Å)	Range (Å)	Exp. time (s)	Telescope (+Instrument)
2013 Jul 27.71	56500.71	−0.17	18	3500–9100	1200	LJT+YFOSC
2013 Jul 31.72	56504.72	+3.84	18	3430–8980	1200	LJT+YFOSC
2013 Aug 02.64	56506.64	+5.76	18	3430–8960	1200	LJT+YFOSC
2013 Aug 03.63	56507.63	+6.75	18	3410–9000	1200	LJT+YFOSC
2013 Aug 09.60	56513.63	+12.75	25	3470–8840	1800	XJT+BFOSC
2013 Aug 13.78	56517.78	+16.90	18	3430–9020	1200	LJT+YFOSC
2013 Aug 17.71	56521.71	+20.83	18	3450–9010	1200	LJT+YFOSC
2013 Aug 23.73	56527.73	+26.85	18	3620–8970	1200	LJT+YFOSC
2013 Sep 12.65	56547.65	+46.77	18	3380–9030	1200	LJT+YFOSC
2013 Sep 25.60	56560.65	+59.77	25	3500–8850	2400	XJT+BFOSC
2013 Sep 29.50	56564.50	+63.62	18	3420–9010	1800	LJT+YFOSC
2013 Oct 04.50	56569.50	+68.62	25	3770–8750	2400	XJT+BFOSC
2013 Nov 02.52	56598.52	+97.64	18	3400–9050	1800	LJT+YFOSC
2013 Nov 14.50	56610.50	+109.62	18	3400–9110	1800	LJT+YFOSC
2013 Nov 16.49	56612.49	+111.61	18	3390–9130	1800	LJT+YFOSC
2013 Nov 29.49	56625.49	+124.61	18	3480–9130	1350	LJT+YFOSC
2013 Dec 03.50	56630.50	+129.62	18	3530–9110	2700	LJT+YFOSC
2013 Dec 20.60	56646.60	+145.72	18	4070–9100	3000	LJT+YFOSC
2013 Dec 23.54	56649.54	+148.66	18	3950–9080	3600	LJT+YFOSC
2014 Jan 04.48	56661.48	+160.60	18	3610–9090	4200	LJT+YFOSC
2014 Jan 23.50	56680.50	+179.62	18	3520–9110	2700	LJT+YFOSC

Note. Journal of spectroscopic observations of SN 2013dy.

^a Relative to the B band maximum on JD. 2456501.38.

$U - B$ color of SN 2013dy is similar to SN 1999aa; both are bluer than the others at $t < +5$ days. It might imply a similar temperature between SN 2013dy and SN 1999aa at this period. A larger scatter appears in the $V - I$ color of SN 2013dy and SN 2011fe at $t > +80$ days.

Figure 5 displays the $uvm2 - uu$ color of SN 2013dy based on the observations of *Swift*-UVOT and corrected for the extinction. Comparisons are made between the normal SN 2011fe (Brown et al. 2012), narrow-lined SN 2012fr (Zhang et al. 2014), 91T-like (Filippenko 1992a; Mazzali et al. 1995) event SN 2007cq (Brown et al. 2014), 99aa-like (Garavini et al. 2004) event iPTF 14bdn (Smitka et al. 2015), 02cx-like (Li et al. 2003) event SN 2005hk (Brown et al. 2014), and UV excess event SN 2011de (Brown 2014). These samples seem to be divided into two groups, where SN 2013dy, SN 2011fe, SN 2012fr, and iPTF 14bdn are located in the upper region with a redder color (i.e., ≥ 3 mag) than the remaining peculiar events (i.e., SN 2007cq, SN 2005hk, and SN 2011de). In general, the color of SN 2013dy is similar to that of iPTF 14bdn at $t > -5$ days. Before this period, iPTF 14bdn turns red monotonically, which is distinct from that of SN 2011fe and SN 2012fr. On the other hand, SN 2013dy presents a flatter curve and is located in the middle of this upper group. This might relate to the transitional position of SN 2013dy in the classification scheme (e.g., located on the border of normal and 91T/99aa-like events), as discussed in Section 5.4.

3.3. Extinction

The reddening due to the host galaxy can be estimated using several empirical methods. For example, the spectra published in Z13 exhibit significant Na I D absorption from both the host galaxy and the Milky Way. On the other hand, we can derive it according to the Lira–Phillips relation based on the intrinsic $B - V$ color at $+30 < t < +90$ days (Phillips et al. 1999).

Additionally, the maximum-light color $B_{\text{max}} - V_{\text{max}}$ related to the decline rate can also be used to estimate the reddening of SNe Ia (e.g., Phillips et al. 1999; Wang et al. 2009a). All of these methods are introduced to calculate the host galaxy reddening of SN 2013dy, as listed in Table 6, and yield an average value $E(B - V)_{\text{host}} = 0.20 \pm 0.10$ mag. Considering the Galactic reddening ($E(B - V) = 0.15 \pm 0.02$ mag), $E(B - V)_{\text{total}} = 0.35 \pm 0.10$ mag is thus adopted in this paper.

4. SPECTRA

4.1. Temporal Evolution

4.1.1. Pre-maximum

Figure 6 displays the selected early spectra of SN 2013dy (Z13). Overplotted are the early spectra of SN 1999aa (Garavini et al. 2004), SN 2003du (Stanishev et al. 2007), SN 2009dc (Taubenberger et al. 2010), SN 2011fe (Nugent et al. 2011; Zhang et al. 2016b), SN 2012fr (Childress et al. 2013; Zhang et al. 2014), and iPTF 14bdn (Smitka et al. 2015) at similar phases.

The early spectra of SN 2013dy consist of the absorption features from singly ionized intermediate-mass elements (IMEs, e.g., Si, S, Mg, and Ca) and Fe, which are usually seen in normal SNe Ia. Note that the absence of Fe III features in the early spectra of SN 2013dy would indicate a lower temperature than 91T/99aa events, which are characterized by the strong absorptions of double-ionized iron (Mazzali et al. 1995).

The first spectrum of SN 2013dy is characterized by the strong absorptions of unburnt carbon of $\text{C II } \lambda 6580$. A weaker $\text{C II } \lambda 7234$ feature is also visible. Though the absorption of $\text{C II } \lambda 6580$ is not rarely seen in the normal SNe Ia (e.g., 25%; Parrent et al. 2011; Silverman & Filippenko 2012), it is usually not strong. Besides of SN 2013dy, such a strong absorption of

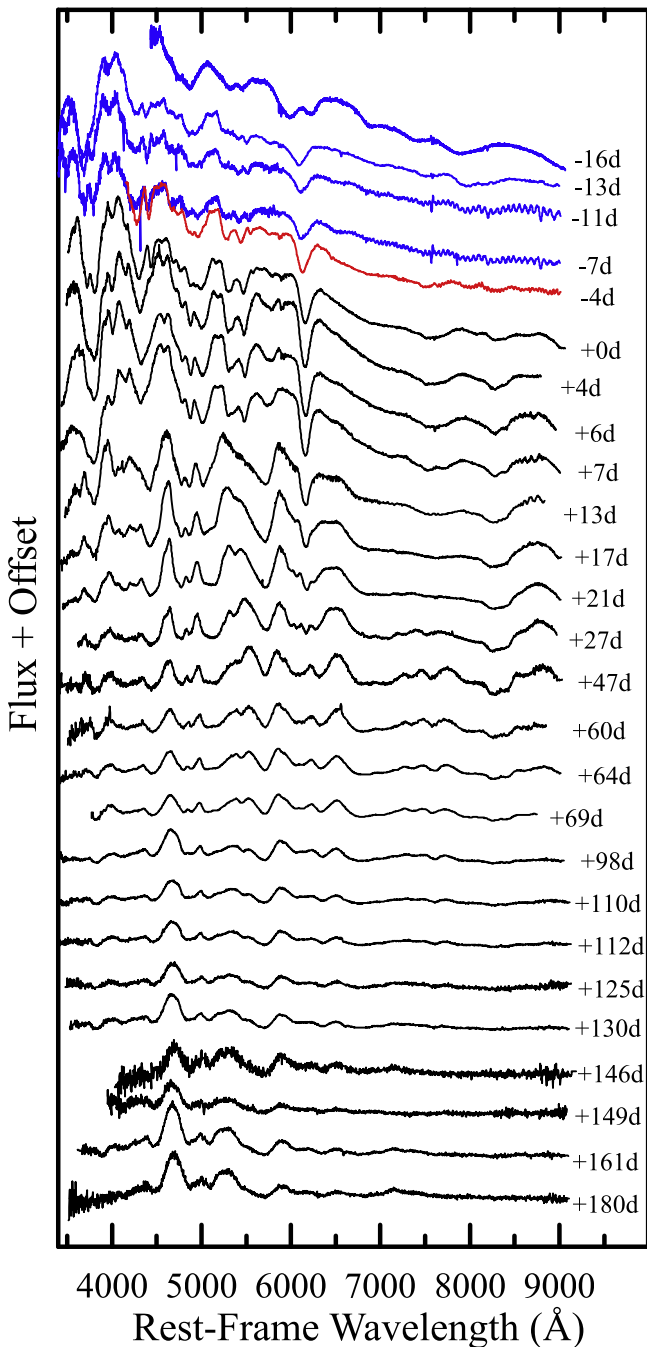


Figure 3. Optical spectra of SN 2013dy from $t \approx -16$ days to $t \approx +180$ days with arbitrary vertical offsets for clarity. The epochs are marked for better display. Note that the spectra at $t < +0$ days are published in Z13 (blue) and P15 (red).

C II $\lambda 6580$ was only found in the superluminous Ia SN 2009dc (Taubenberger et al. 2010). The spectrum of the very young SN 2011fe at $t \approx -16$ days exhibits rather weaker C II than that of SN 2013dy. On the other hand, the C II $\lambda 6580$ line in SN 2013dy weakens rapidly, and most of the other SNe Ia are not obtained as early as this SN. In fact, three days later, the strength of the C II $\lambda 6580$ line in SN 2013dy becomes as weak as that of SN 2003du at the same phase.

Note that the equivalent width (EW) ratio of C II $\lambda 6580$ and Si II $\lambda 6355$ in the spectrum of SN 2013dy at $t \approx -16$ days is $R(C/Si) = 0.48 \pm 0.04$, which is similar to that of SN 2009dc at

Table 5
UV and Optical Light Curve Parameters of SN 2013dy

Band	λ_{eff} (Å)	$t_{\text{max}}^{\text{a}}$	$m_{\text{peak}}^{\text{b}}$ (mag ^b)	Δm_{15}^{b} (mag ^b)	$M_{\text{peak}}^{\text{b}}$ (mag ^b)
<i>uvw2</i> ^c	1928	498.07(40)	17.62(10)	2.49(20)	-16.90(60)
<i>uvm2</i>	2246	499.74(60)	17.65(08)	1.47(12)	-16.34(50)
<i>uvw1</i> ^c	2600	498.39(50)	14.47(10)	2.50(20)	-19.14(60)
<i>U</i>	3650	498.98(30)	12.88(05)	1.35(08)	-20.34(45)
<i>B</i>	4450	500.88(30)	13.29(01)	0.90(03)	-19.65(40)
<i>V</i>	5500	501.87(30)	12.94(01)	0.57(03)	-19.62(40)
<i>R</i>	6450	501.45(30)	12.83(02)	0.54(03)	-19.62(40)
<i>I</i>	7870	498.72(30)	12.95(02)	0.47(03)	-19.54(40)
<i>Y</i> ^d	9100	496.00(40)	13.58(04)	0.97(05)	-18.42(35)
<i>J</i> ^d	12500	499.37(30)	13.80(03)	1.69(05)	-18.02(35)
<i>H</i> ^d	16000	496.41(30)	14.37(03)	0.39(05)	-17.33(30)

Notes.

^a Uncertainties of peak-light dates, in units of 0.01 days, are 1σ . The date is MJD-56000.

^b Uncertainties of magnitudes, in units of 0.01 mag, are 1σ .

^c The estimations of *uvw2* and *uvw1* are corrected for the “Red tail” of each filter (Brown et al. 2010).

^d Based on the NIR photometry published in P15.

$t \approx -10$ days (i.e., ~ 0.50). It might imply a similar abundance of unburnt carbon in these two SNe Ia. However, the velocity distribution of C II $\lambda 6580$ in SN 2013dy is $5700 \pm 200 \text{ km s}^{-1}$ and larger than that of SN 2009dc (i.e., $\sim 4000 \text{ km s}^{-1}$), which might indicate a wider distribution of unburnt carbon in the outer ejecta of the former.

At this phase, the blue-side absorption feature, the so-called high velocity features (HVFs; e.g., Mazzali et al. 2005a, 2005b), are gradually weakened in Ca II (i.e., H&K and IR triplet) with the emergence of the photometric component. The HVF of the Ca II IR triplet in the spectra of SN 2013dy begins at $v \approx 26,000 \text{ km s}^{-1}$. Such an HVF is similarly seen in SN 2003du, SN 2011fe, and SN 2012fr. There is no evidence for the detached-HVF component of Si II $\lambda 6355$ in the spectrum of SN 2013dy at $t \approx -16$ days. Two days later, the profile of Si II $\lambda 6355$ becomes non-Gaussian, which might indicate two departing components in this absorption, and the bluer one should be the HVF of Si II.

At around $t \approx -7$ days, the spectrum of SN 2013dy resembles to that of the 99aa-like event iPTF 14bdn, especially for the profile of Ca II H&K and IR triplets, which are weaker than that in SN 2003du, SN 2011fe, and SN 2012fr. Additionally, the strength of Si II $\lambda 6355$ in the spectrum of SN 2013dy is also weaker than in SN 2003du and SN 2011fe. It might indicate that the temperature of SN 2013dy is higher than that of SN 2003du and SN 2011fe, since a higher temperature might reduce the abundance of IMEs and reproduce the observed weakening of the IME lines in objects (Mazzali et al. 1995).

4.1.2. Around Maximum

Figure 7 displays the spectra of SN 2013dy in the first week after the *B* band maximum compared with that of SN 1999aa (Garavini et al. 2004), SN 2003du (Stanishev et al. 2007), SN 2011fe (Pereira et al. 2013), and SN 2012fr (Zhang et al. 2014).

In general, the spectra of SN 2013dy resemble that of SN 1999aa at $t \approx +0$ days. At this phase, the absorption feature of Si II $\lambda 6355$ evolves to be the dominant feature in normal profile.

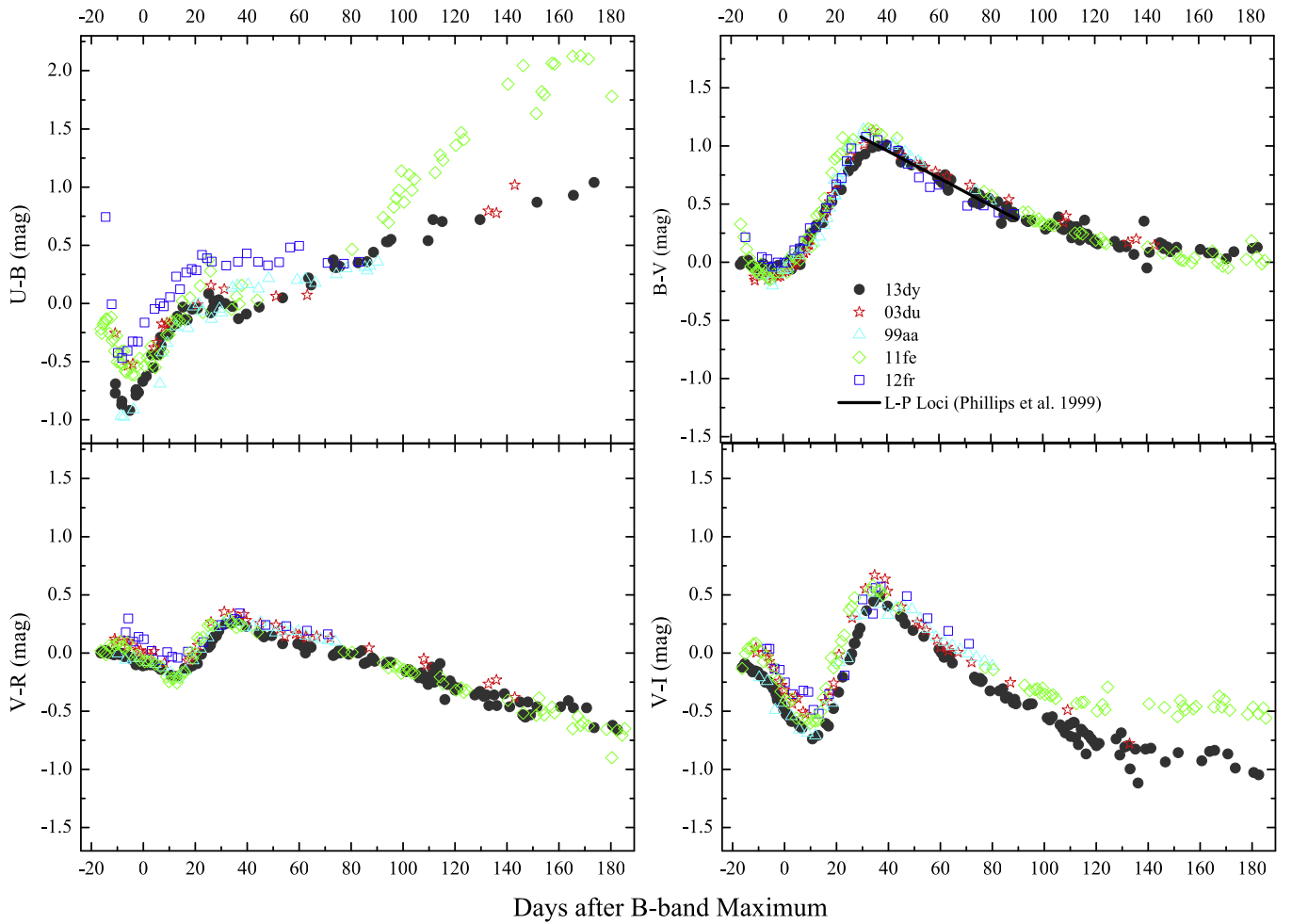


Figure 4. Optical color curves of SN 2013dy compared with those of SN 1999aa, SN 2003du, SN 2011fe, and SN 2012fr; see the text for details.

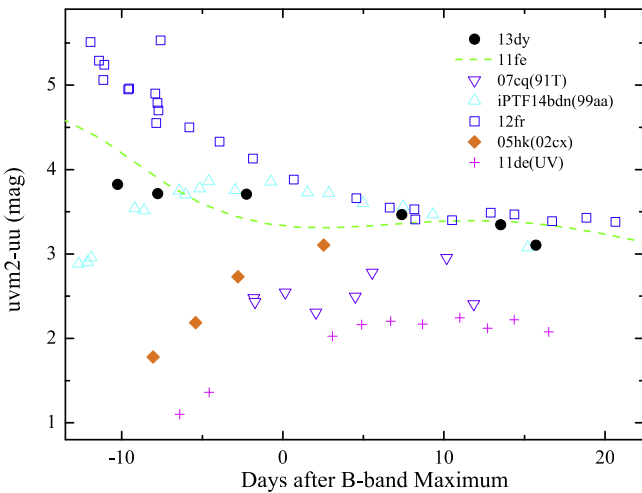


Figure 5. $uvm2 - uu$ color curve of SN 2013dy compared with that of SN 2011fe (normal), SN 2012fr (narrow-lined), SN 2007cq (91T-like), iPTF 14bdn (99aa-like), SN 2005hk (02cx-like), and SN 2011de (UV excess); see the text for details.

A minor absorption on the blue side of Na I D is likely due to Si II $\lambda 5972$, which is absent in the early spectra. The line-strength ratio of Si II $\lambda 5972$ to Si II $\lambda 6355$, known as $R(\text{Si II})$ (Nugent et al. 1997), is an approximated indicator of the photospheric temperature, with a larger value corresponding to

Table 6
The Host Extinction of SN 2013dy

Method	Details	Results (mag)
EW(Na I D) ^a	0.16EW-0.01 ^b	0.07 ± 0.05
EW(Na I D) ^a	0.51EW-0.04 ^b	0.23 ± 0.05
EW(Na I D) ^a	0.43EW-0.08 ^c	0.15 ± 0.05
Color curve	$B_{\max} - V_{\max}$ ^d	0.32 ± 0.05
Color curve	Lira-Phillips ^e	0.20 ± 0.05

Notes.

^a $\text{EW}(\text{Na I D}) = 0.53 \text{ \AA}$, estimated by Z13.

^b Turatto et al. (2003).

^c Poznanski et al. (2011).

^d Wang et al. (2009b).

^e Phillips et al. (1999).

a lower temperature and smaller $\Delta m_{15}(B)$ (Hachinger et al. 2006).

The ratio between Si II $\lambda 5972$ and Fe II near $\sim 4800 \text{ \AA}$ (marked as $R[\text{Si}/\text{Fe}]$) shows a constant relation to the $\Delta m_{15}(B)$ (e.g., Hachinger et al. 2006). Hachinger et al. (2006) also suggested that the ratios of $\text{EW}(\text{Si II } \lambda 6355)$ and $\text{EW}(\text{S II})$, known as the “w” feature) to $\text{EW}(\text{Fe II})$, marked as $R(\text{Si}/\text{Fe})$ and $R(\text{S}/\text{Fe})$, respectively, might indicate the intrinsic temperature and brightness of SNe Ia. The behavior for the S II could be explained as the effect of increasing temperature, and

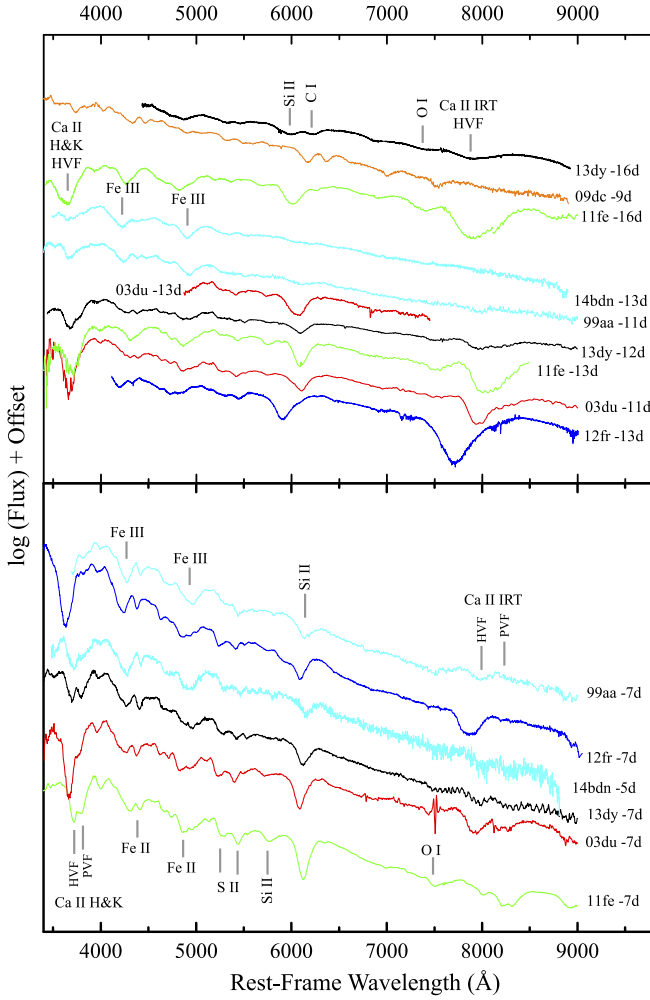


Figure 6. Early spectra of SN 2013dy overplotted with the spectra of SN 1999aa, SN 2003du, SN 2009dc, SN 2011fe, SN 2012fr, and iPTF 14bdn at the selected phases. All of these spectra were corrected with redshift and reddening.

the ratio between Si and Fe might reflect an abundance change. The SNe Ia with the smallest decline rates (e.g., $\Delta m_{15}(B) \leq 1.0$ mag) have more Fe near the maximum-light photosphere ($\sim 10,000$ km s $^{-1}$) and the intermediate decliners have more IME and less Fe at a similar velocity (Mazzali et al. 2007). We note that the explosion velocity of SN 2013dy, SN 1999aa, SN 2003du, and SN 2011fe are similar and close to $\sim 10,000$ km s $^{-1}$ at around peak brightness. Thus, we can compare the temperature, brightness, and the mass of Fe in these SNe Ia through the $R(S/Fe)$ and $R(Si/Fe)$. The $R(Si)$, $R(S/Fe)$, $R[Si/Fe]$, and $R(Si/Fe)$ at $t \approx +0$ days for the selected sample are measured and listed in Table 7. We find that the relations of $\Delta m_{15}(B)$ and the EW ratios of our sample generally conform to the research of Hachinger et al. (2006). The smaller $R(Si \text{ II})$ and $R(S/Fe)$ of SN 2013dy tend to indicate a higher temperature for this SN than that of the comparisons at $t \approx +0$ days. Moreover, this table might suggest a similar mass of Fe and brightness in SN 2013dy and SN 1999aa, which are larger than those in SN 2003du and SN 2011fe.

A notable distinction among SN 2013dy and the comparison SNe is the profile of the absorptions around 3800 Å, which can be attributed to the absorptions of Ca II H&K. Such a difference might relate to the scatters in the $U - B$ color, and the behavior

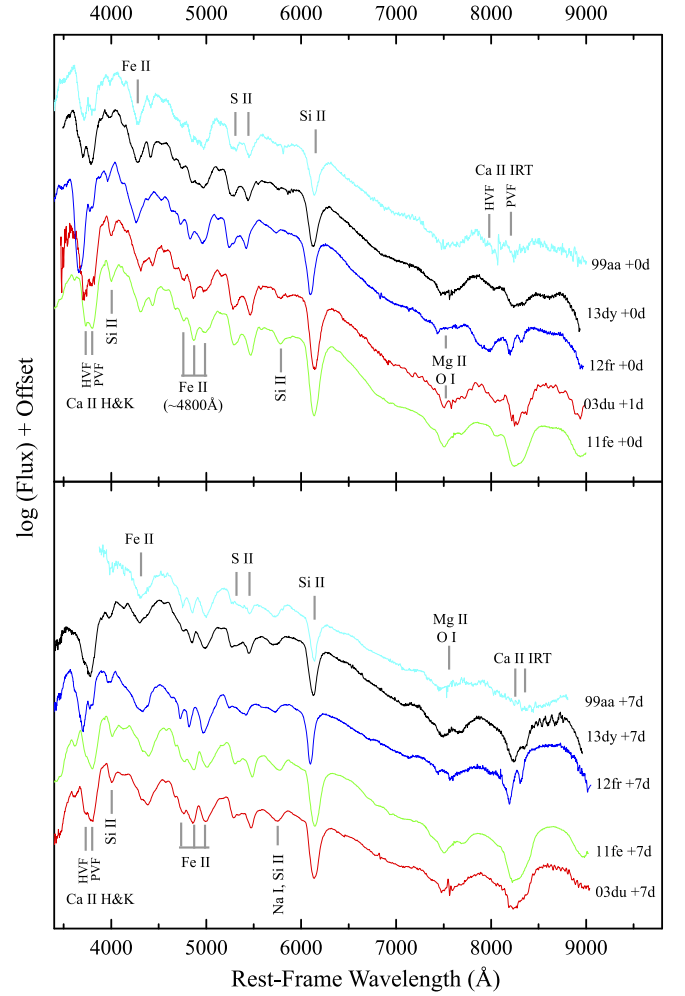


Figure 7. Spectra of SN 2013dy, SN 2012fr, SN 2011fe, SN 2003du, and SN 1999aa around maximum. All of these spectra were corrected with redshift and reddening.

Table 7
Parameters for the $\Delta m_{15}(B) - EW$ Ratio Relation

SN	Δm_{15}	$R(Si \text{ II})^a$	$R(S/Fe)^b$	$R[Si/Fe]^c$	$R(Si/Fe)^d$
2013dy	0.90	0.05	0.46	0.02	0.48
1999aa	0.83	0.07	0.55	0.04	0.58
2012fr	0.85	0.07	...	0.03	...
2003du	1.02	0.11	0.64	0.08	0.69
2011fe	1.10	0.14	0.68	0.11	0.74

Notes.

^a $EW(Si \text{ II } \lambda 5972)/EW(Si \text{ II } \lambda 6355)$.

^b $EW(S \text{ II "w"})/EW(Fe \text{ II } \sim 4800 \text{ \AA})$.

^c $EW(Si \text{ II } \lambda 5972)/EW(Fe \text{ II } \sim 4800 \text{ \AA})$.

^d $EW(Si \text{ II } \lambda 6355)/EW(Fe \text{ II } \sim 4800 \text{ \AA})$.

of Ca II H&K at maximum light may be an indicator of intrinsic SN Ia color (Chotard et al. 2011; Foley et al. 2011; Blondin et al. 2012; Foley 2012). Based on these samples, we find that the SNe Ia with stronger HVFs of Ca II H&K are usually redder in $U - B$ color around peak brightness.

4.1.3. A Few Months After Maximum

At $t \sim +3$ weeks (see the upper panel of Figure 8), the absorption of Si II $\lambda 6355$ of all the comparison SNe are

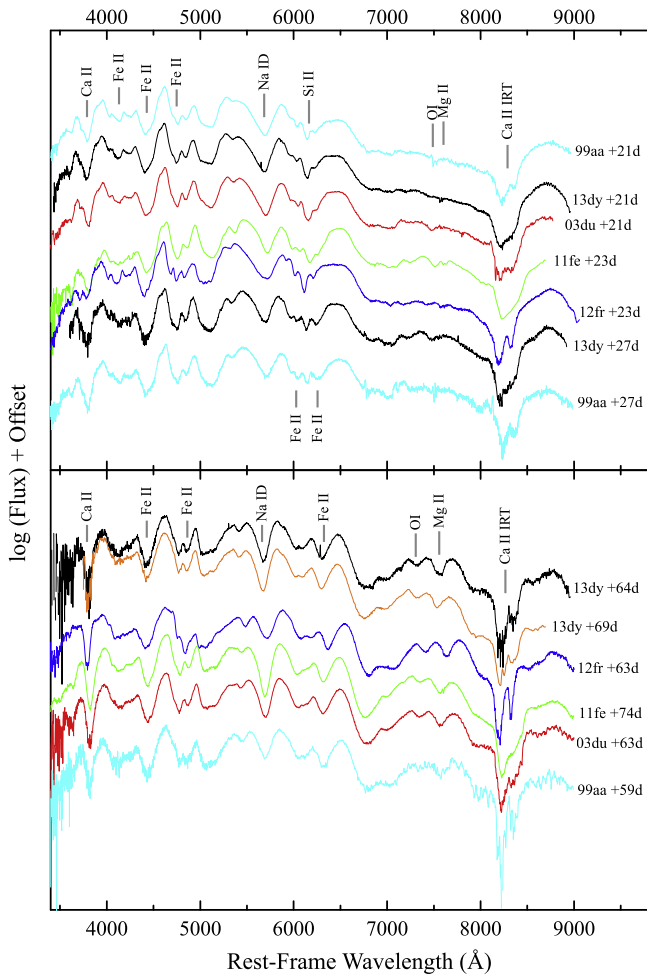


Figure 8. Spectra of SN 2013dy, SN 1999aa, SN 2003du, SN 2011fe, and SN 2012fr at a few months after maximum. All of these spectra were corrected with redshift and reddening.

contaminated by the surrounding absorption of iron-group elements. The spectra features decrease from the maximum and are dominated by the absorption of Na I D. Around $\sim +2$ to $\sim +3$ months after maximum, these spectra become stable without obvious evolution, while the iron-group elements become dominant. One interesting feature is the Ca II IR triplet feature at $t \approx +69$ days, where this triplet is clearly split into three components.

Note that the velocities of Ca II are similar to those of SN 2003du and SN 2011fe but slower than that of SN 2012fr. However, the absorptions of Na I D, O I, and Mg II appear to be faster in the former three SNe Ia than in the latter. This might suggest that the ejecta of SN 2013dy, SN 2003du, and SN 2011fe are well mixed, and a stratification structure might exist in the ejecta of SN 2012fr.

At $t > +4$ months, as presented in Figure 9, all of these samples become uniform and are dominated by the emission of iron-group elements. However, the difference can be found in the strength of some features, for example, the bump from 7000 to 7400 Å, which can contribute to the emission of [Fe II] $\lambda 7155$ and [Ni II] $\lambda 7378$ at $v \sim 2000 \text{ km s}^{-1}$. Such a bump might indicate that SN 2013dy is approaching the nebular phase.

In summary, the above comparisons suggest that SN 2013dy shares major similarities with the normal SN Ia 2003du and SN 2011fe. On the other hand, the spectra of SN 2013dy are also

very similar to those of SN 1999aa and iPTF 14bdn from one week before *B* band maximum.

4.2. Velocities of Ejecta

Figure 10 displays the ejecta velocities of SN 2013dy via the absorption features of some spectral lines, such as Ca II H&K, Si II $\lambda 4130$, Si II $\lambda 5633$, Si II $\lambda 6355$, C II $\lambda 6580$, C II $\lambda 7234$, and the Ca II IR triplet. The location of the absorption minimum was measured using both the Gaussian fit routine and the direct measurement of the center of the absorption, and the results were averaged.

The HVF of the Ca II IR triplet at $t \approx -16$ days is $\sim 26,000 \text{ km s}^{-1}$ which is close to that of SN 2011fe at the same phase and slower than that of SN 2012fr at $t \approx -14$ days (i.e., $\sim 31,000 \text{ km s}^{-1}$; Childress et al. 2013). At this phase, the velocity of Si II $\lambda 6355$ is $\sim 17,200 \text{ km s}^{-1}$ slower than that of the photospheric component of the Ca II IR triplet (i.e., $\sim 20,000 \text{ km s}^{-1}$) and faster than that of the C II features (i.e., $\sim 16,300 \text{ km s}^{-1}$ and $\sim 15,000 \text{ km s}^{-1}$ for $\lambda 6580$ and $\lambda 7234$, respectively). Three days later, the velocity of C II $\lambda 6580$ drops to about $13,000 \text{ km s}^{-1}$, which is close to the typical expansion velocity of this line in SNe Ia (Silverman & Filippenko 2012). It is notable for the velocity plateaus of the HVFs of Ca II from $t \approx -14$ to -6 days at $v \approx 20,000 \text{ km s}^{-1}$, while the velocities of photospheric components (e.g., Ca II and Si II) are quickly declining.

After the maximum light, the velocity of Si II $\lambda 6355$ is $v \sim 10,450 \text{ km s}^{-1}$ with a velocity gradient of $18 \pm 20 \text{ km s}^{-1} \text{ day}^{-1}$. This gradient is derived from the velocity from $t \approx +0$ to $+13$ days and this line is not contaminated by the surrounding lines. Such a low velocity gradient is similarly seen for the velocity evolution of Ca II, which puts SN 2013dy into the LVG category of SNe Ia according to the classification scheme of Benetti et al. (2005). On the other hand, the velocity of Si II $\lambda 5633$ is slower but declines quicker. The IMEs of SN 2013dy generally have similar expansion velocities (e.g., $\sim 10,000 \text{ km s}^{-1}$), suggestive of a relatively uniform distribution of the burning products in the ejecta.

5. DISCUSSION

5.1. Distance

The observed velocity of NGC 7250 is 1166 km s^{-1} , which after correcting for the local group infall onto Virgo, Galaxy, and Shapley becomes 1410 km s^{-1} (Mould et al. 2000) or a distance $D = 19.58 \pm 2.0 \text{ Mpc}$ on the scale of $H_0 = 72 \text{ km s}^{-1} \text{ Mpc}^{-1}$. On the other hand, the distance derived from the Tully–Fisher relation of this galaxy is $D = 13.7 \pm 3.0 \text{ Mpc}$ (Tully et al. 2009; Nasonova et al. 2011), which was adopted in Z13 and P15 as the distance of SN 2013dy. Furthermore, we can calculate the distance from the WLR of SNe Ia (Phillips 1993; Blondin et al. 2012). The brightness of SNe Ia in the *H* band is relatively insensitive to the reddening and is more uniform around the peak compared to the corresponding values in the optical bands (Meikle 2000; Krisciunas et al. 2004; Barone-Nugent et al. 2012). Thus, we can estimate the distance to SN 2013dy based on its *H* band light curve published in P15.

Table 8 lists the distance derived from the above methods and an average value $D = 20.0 \pm 4.0 \text{ Mpc}$ is adopted. Note that the estimation from the *H* band brightness (i.e., $D = 31.3 \pm 3.0 \text{ Mpc}$) is much larger than that inferred from

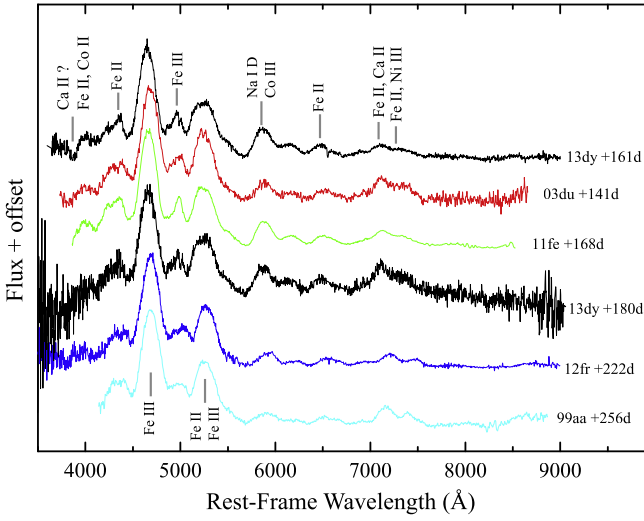


Figure 9. Spectra of SN 2013dy, SN 1999aa, SN 2003du, SN 2011fe, and SN 2012fr (Childress et al. 2015) near the nebular phase. These spectra are normalized accordingly based on the region of 4400–5000 Å. All of these spectra were corrected with redshift and reddening.

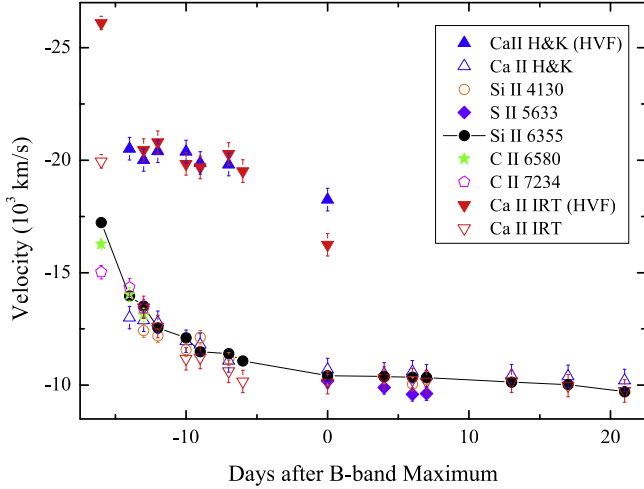


Figure 10. Velocity evolution of different elements inferred from the spectra of SN 2013dy.

Table 8
Estimations for the Distance of SN 2013dy

Method	Details	Results (Mpc)
Hubble Flow ^a	1410 km s ⁻¹	19.6 ± 2.0
Tully–Fisher ^b	<i>JHK</i> bands	13.7 ± 3.0
Phillips Relation ^c	$\Delta m_{15}(B) = 0.90$	17.0 ± 3.0
Phillips Relation ^d	$\Delta m_{15}(B) = 0.90$	19.5 ± 3.0
NIR luminous ^e	<i>H</i> band	31.3 ± 3.0 ^f

Notes.

^a Corrected for Virgo infall, GA, and Shapley (Mould et al. 2000), on the scale of $H_0 = 72 \text{ km s}^{-1} \text{ Mpc}^{-1}$.

^b Tully et al. (2009) and Nasonova et al. (2011).

^c $\Delta m_{15}(B) = 0.90$; Phillips (1993).

^d Modified Phillips (1993) relation from Figure 13 of Blondin et al. (2012) for the normal SNe Ia.

^e From the *H* band light curve of SN 2013dy published by P15

^f The error of extinction is involved.

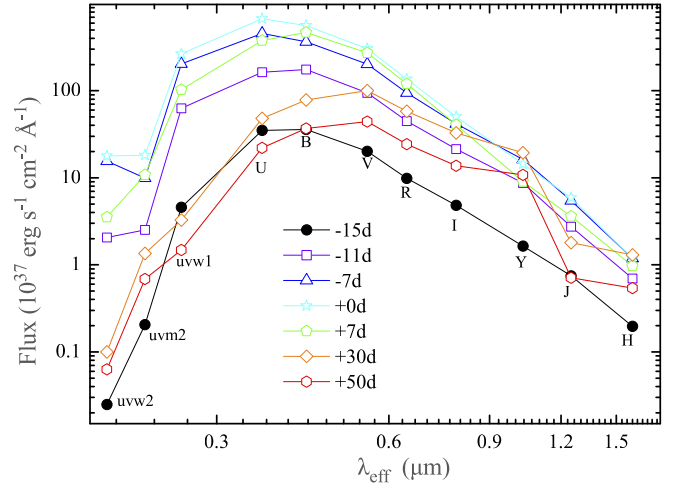


Figure 11. Spectral energy distribution of SN 2013dy at $t \approx -14, -11, -7, +0, +7, +30,$ and $+50$ days. The positions of effective wavelength for each filter are marked.

other methods. It suggests that the intrinsic *H* band brightness of SN 2013dy (i.e., $M(H) = -17.33 \pm 0.24$ mag, if $D = 20.0$ Mpc or $M(H) = -16.51 \pm 0.24$ mag if $D = 13.7$ Mpc) is at least 1.0 mag lower than the normal (e.g., $M(H) = -18.432 \pm 0.017$ mag, Kattner et al. 2012; -18.40 ± 0.08 mag, Folatelli et al. 2010; -18.30 ± 0.04 mag, Barone-Nugent et al. 2012; -18.314 ± 0.024 mag, Weyant et al. 2014). Besides, Zhang et al. (2016a) pointed out that the peak *H* band brightness of SN 2011hr (an extreme 91T-like event, $\Delta m_{15}(B) = 0.93$ mag) is about 0.7 mag higher than the average. Therefore, the scatter of SNe Ia in the *H* band is about 2.0–2.5 mag for the SNe Ia with small decline rates (i.e., $\Delta m_{15}(B) \approx 0.90$). This larger scatter might be a challenge to the assumption that the NIR luminosities are more uniform in SNe Ia.

5.2. Spectral Energy Distribution

Based on the UV, optical, and NIR photometry (covering the wavelength from 1600 to 18000 Å) presented in Figure 2, we can construct the SED of SN 2013dy roughly through the observed fluxes in various passbands at the same epochs. The missing data can be obtained through interpolation of the adjacent data. Figure 11 displays the SED of SN 2013dy at $t \approx -15, -11, -7, +0, +7, +30,$ and $+50$ days. Note that the *uvw2* and *uvw1* fluxes are corrected for the “red tail” effect (Brown et al. 2010). This figure shows a clear energy translation of SN 2013dy from blue to red in wavelength. A notable bump around the *Y* band at $t \geq +30$ days might relate to the deficit in the *J* and *H* bands.

To understand the energy transmission of SN 2013dy, we compare its SED with that of SN 2003du, SN 2011fe, SN 2012fr, and iPTF 14bdn at six selected phases; see Figure 12. It is notable that the NIR fluxes of SN 2013dy are much lower than those in SN 2003du and SN 2011fe. The lower flux of SN 2013dy in the *J* and *H* bands conforms to the bluer $V - J$ and $V - H$ color compared to those in SN 2011fe, as reported in Figure 5 of P15.

The SED could give a limit to the extinction of these SNe Ia. For example, the temperature of SN 2013dy should be lower

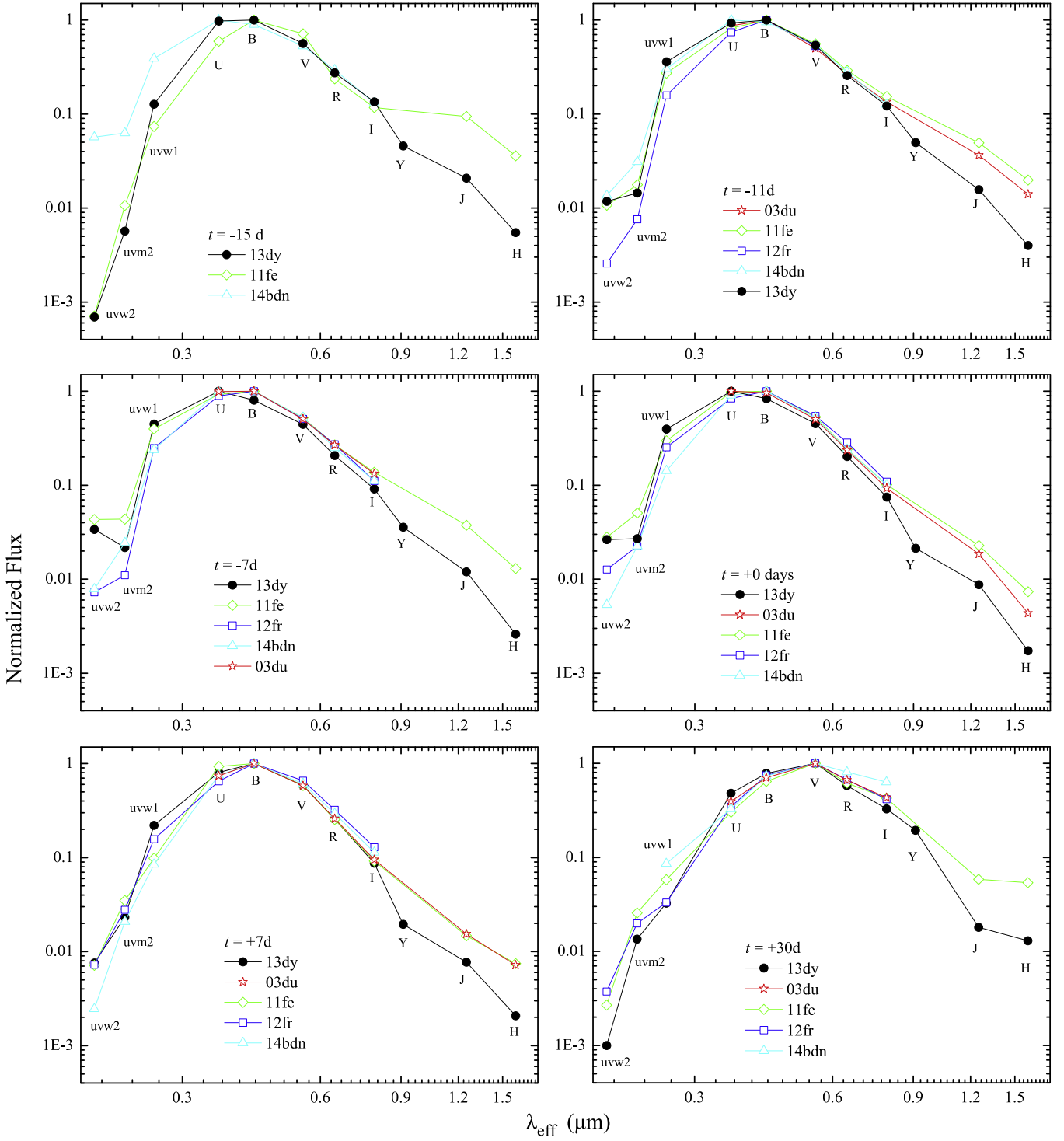


Figure 12. SED Comparison for SN 2003du, SN 2011fe, SN 2012fr, SN 2013dy, and iPTF 14bdn (99aa-like) at $t \approx -15, -11, -7, +0, +7,$ and $+30$ days.

than that of iPTF 14bdn at $t < -7$ days owing to the absence of Fe III lines in the spectra of the former. On the other hand, SN 2013dy might have a higher temperature than that of SN 2003du and SN 2011fe in light of the comparison of spectral features. Furthermore, the reddenings of SN 2003du, SN 2011fe, and iPTF 14bdn are quite small (e.g., $E(B - V) < 0.03$). The sequence of temperature could give a region of extinction, i.e., $0.20 \leq E(B - V) \leq 0.30$, which conforms to the estimation in Section 3.3.

5.3. Bolometric Light Curve and the Mass of ^{56}Ni

Figure 13 displays the quasi-bolometric light curves of SN 2013dy derived from *UBVRI* photometry, compared with that of SN 1999aa, SN 2003du, SN 2011fe, and SN 2012fr. SN 2013dy is similar to SN 2012fr but with slightly higher luminosity.

We calculate the UV–optical–NIR (“uvoir,” covering the wavelength from 1600 Å to 24000 Å) bolometric light curves of SN 2013dy at $-15 < t < +50$ days based on the

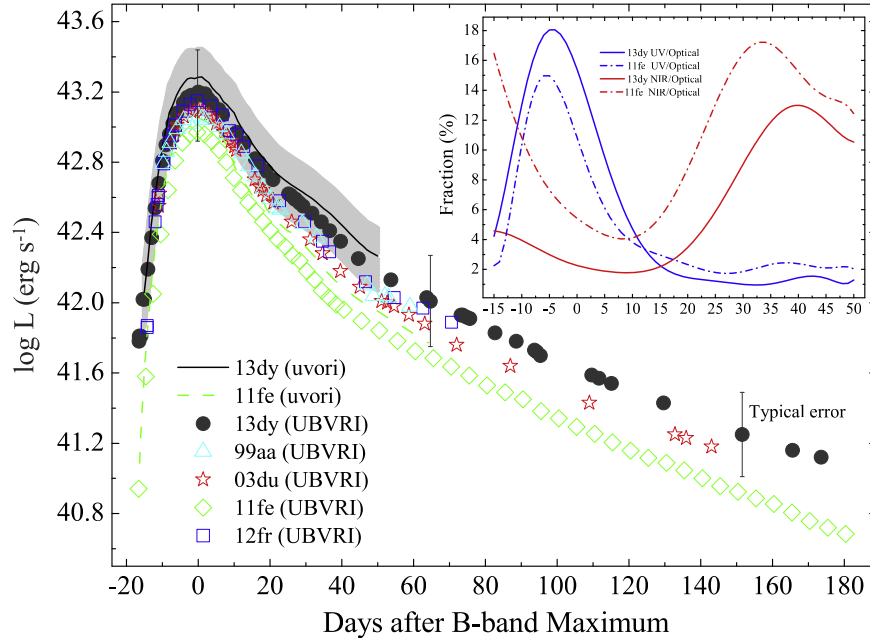


Figure 13. Quasi-bolometric *UBVR* (3300–9000 Å) light curves of SN 2013dy compared with that of SN 1999aa, SN 2003du, SN 2011fe, and SN 2012fr. The “uvoir” (1600–24000 Å) of SN 2013dy and SN 2011fe are overlotted. The gray area shows the 1σ range of the “uvoir” bolometric luminosities of SN 2013dy considering the uncertainties from the distance (i.e., $D = 20.0 \pm 4.0$ Mpc). The fraction of UV (1600–3300 Å) and NIR (9000–24000 Å) flux to the optical flux for SN 2013dy and SN 2011fe are presented in the top right panel.

photometry presented in Figure 2. Note that the UV flux at $t < -10$ days is estimated through the stretched UV light curves of SN 2011fe, which might induce some errors because of the difference presented in Figure 5. The fluxes beyond the *H* band (i.e., 18000 to 24000 Å) are extrapolated through blackbody approximation. The missing fluxes at wavelengths shorter than the *Swift* UV filters (e.g., < 1600 Å) or longer than 24000 Å are negligible. The “uvoir” bolometric light curve of SN 2011fe (Zhang et al. 2016b) is also overlotted in this figure. An obvious shoulder around $t \approx +40$ days of SN 2013dy implies a higher intrinsic luminosity than SN 2011fe.

The fraction of the UV (1600–3300 Å) and NIR (9000–24000 Å) to the optical flux of SN 2013dy and SN 2011fe is presented in the top right panel of Figure 13. Based on this panel, we find that the UV flux of SN 2013dy is relatively higher than that of SN 2011fe at the early phase while the NIR flux of the former is relatively lower. It also indicates that SN 2013dy has relatively stronger optical flux at $t > \sim +10$ days.

Based on the “uvoir” light curve, we estimate that SN 2013dy reaches its bolometric maximum ($L_{\max} = 1.95 \pm 0.55 \times 10^{43}$ erg s⁻¹) at about 0.9 days before the *B* band maximum. This could also be found in some bright SNe Ia (e.g., 91T/99aa-like events) and relates to the strong contribution at wavelengths shorter than the *B* band. The uncertainty of the peak flux includes the errors in the distance modulus, the observed magnitudes, the NIR corrections, and missing flux. Z13 found that the first-light time of SN 2013dy is JD 2456483.18, thus the rise time of the bolometric light curve (i.e., $t_{\text{rise}} \approx 17.3$ days) is adopted in the following estimation. With the derived bolometric luminosity and the rise time of the bolometric light curve, the synthesized ⁵⁶Ni mass estimated using the Arnett law (Arnett 1982; Stritzinger & Leibundgut 2005) is $M(^{56}\text{Ni}) = 0.90 \pm 0.26 M_{\odot}$. This value is similar to that of SN 2012fr ($0.88 M_{\odot}$, Zhang et al. 2014) and larger than that of SN 1999aa ($0.72 M_{\odot}$, this paper), SN 2003du

(i.e., $0.63 \pm 0.19 M_{\odot}$, this paper; $0.68 M_{\odot}$, Stanishev et al. 2007; $0.60 M_{\odot}$, Stritzinger et al. 2006), and SN 2011fe (e.g., $0.53 M_{\odot}$, Munari et al. 2013; $0.56 M_{\odot}$, Mazzali et al. 2014).

On the other hand, we could estimate some explosion parameters of this SN by adopting the same method as in Taubenberger et al. (2010). The ejecta mass (M_{ej}) and the total explosion energy (E_{ej}) can be derived from the diffuse time τ_{m} and ejecta velocity v , where $M_{\text{ej}} \propto \tau_{\text{m}}^2 v$ and $E_{\text{kin}} \propto \tau_{\text{m}}^2 v^3$. The diffuse time of SN 2013dy is 27.58 days, which is longer than that of SN 2011fe (i.e., 25.33 days). On the other hand, the velocity of Si II $\lambda 6355$ of SN 2013dy at around maximum is $10,450$ km s⁻¹, which is also slightly faster than that of SN 2011fe (i.e., $10,340$ km s⁻¹). As a result, we find that $M_{\text{ej},13\text{dy}} \approx 1.20 M_{\text{ej},11\text{fe}}$ and $E_{\text{ej},13\text{dy}} \approx 1.22 E_{\text{ej},11\text{fe}}$. Note that these coefficients conform to the stretch factors adopted in Figure 2 for the light curve comparison. The mass of ⁵⁶Ni produced in SN 2013dy is $0.67 M_{\odot}$ based on the estimation of SN 2011fe (e.g., $0.56 M_{\odot}$, Mazzali et al. 2014) and the similar component assumption in Arnett’s (1982) law. This result is independent of distance and extinction. It is smaller than the estimation of the bolometric curve. A smaller estimation for the ⁵⁶Ni mass of SN 2013dy might suggest a distinct energy and material distribution between SN 2013dy and SN 2011fe since only the opaque mass can be calculated from these simple analytic approaches.

5.4. Spectroscopy Classification

Spectroscopy classification schemes have recently been proposed to highlight the diversity of relatively normal SNe Ia. Benetti et al. (2005) classified the normal SNe Ia into LVG and HVG groups by the temporal velocity gradient of the Si II $\lambda 6355$ line. Based on the EW of the absorption features of Si II $\lambda 5972$ and Si II $\lambda 6355$, Branch et al. (2006, 2009) suggested dividing the SN Ia sample into four groups: cool

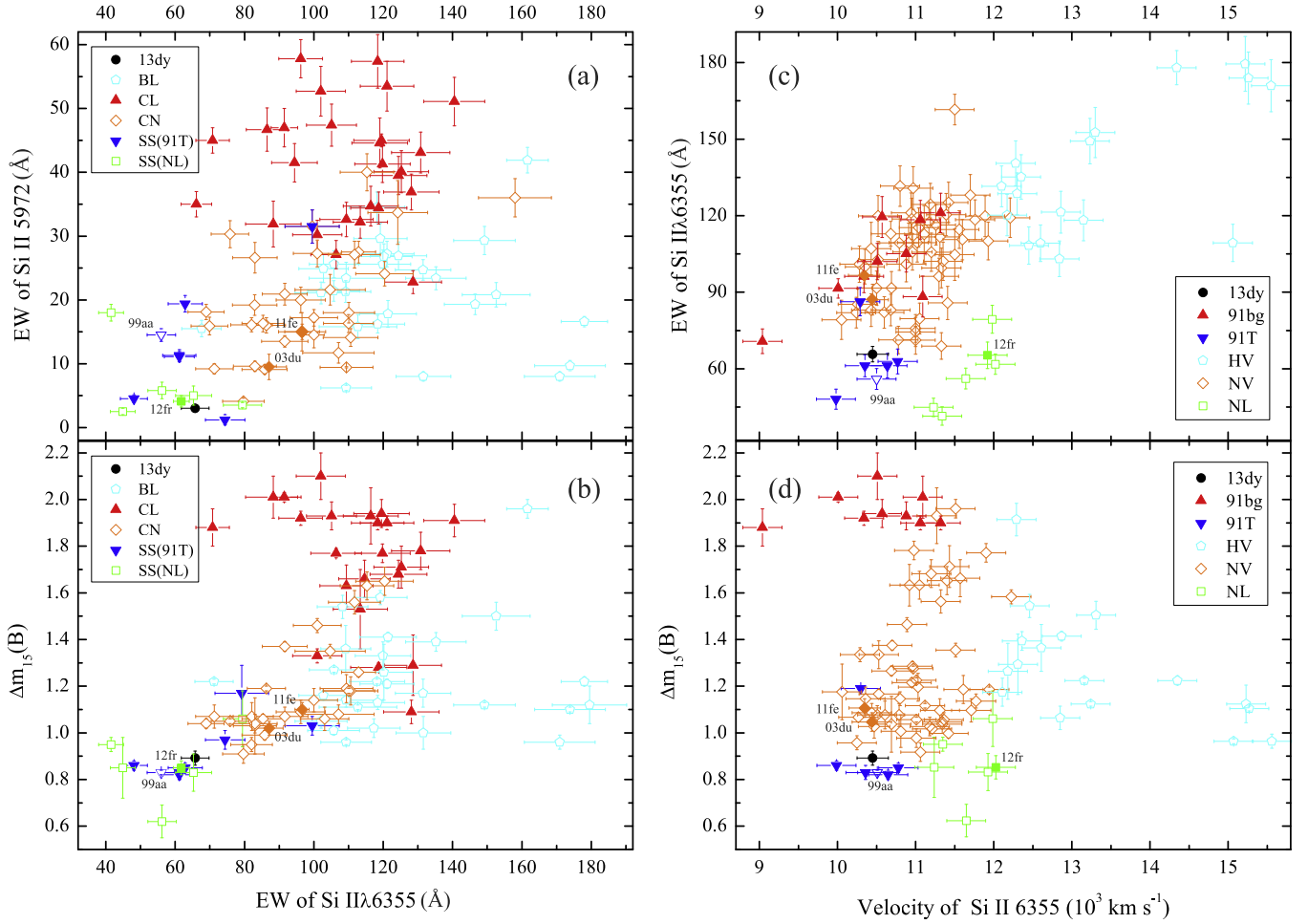


Figure 14. Comparison of various spectroscopic and photometric indicators from SN 2013dy with those from other SNe Ia as measured by Blondin et al. (2012), Silverman et al. (2012), Wang et al. (2009a), Zhang et al. (2014), and this paper. The selected sample have spectra within $t \pm 3$ days. Panel (a) and (b): the Si II $\lambda 5972$ and $\Delta m_{15}(B)$ vs. Si II $\lambda 6355$ at maximum light with subclasses defined by Branch et al. (2009); panel (c) and (d): the EW of Si II $\lambda 6355$ and $\Delta m_{15}(B)$ vs. the velocity of Si II 6355 at maximum light with subclasses defined by Wang et al. (2009a).

(CL), shallow silicon (SS), core normal (CN), and broad line (BL). The CL group mainly consists of the faint objects like SN 1991bg (Filippenko 1992b). Besides the faint peculiar events like SN 2002cx (Li et al. 2003), the SS group mainly consists of the bright 91T/99aa-like events, the superluminous events (e.g., SN 2003fg, Howell et al. 2006; SN 2007if, Scalzo et al. 2010 and SN 2009dc, Taubenberger et al. 2010; Silverman et al. 2011), and the narrow-lined SNe Ia (NL; e.g., SN 2012fr; Zhang et al. 2014). We note that the small EW of Si II $\lambda 6355$ could be derived from different profiles of this line, for example, absorption with smaller depth and larger width (e.g., 91T/99aa-like events) or with larger depth and small width (e.g., NL). Therefore, we divide the bright but generally normal members of SS into two subgroups, SS/91T-like and SS/NL, in the following discussion. On the other hand, Wang et al. (2009a) proposed using the expansion velocity of the Si II $\lambda 6355$ line to distinguish the subclass with a higher Si II velocity (HV) from that with a normal velocity (NV). The HV SNe Ia are found to have redder $B - V$ colors (Wang et al. 2009a) and different locations within host galaxies in comparison to the NV ones (Wang et al. 2013), suggesting that the properties of their progenitors may be different.

The spectroscopy classification of SN 2013dy is compared with the large SNe Ia sample from the spectral data sets of CfA (Blondin et al. 2012) and the Berkeley SuperNova Ia

Program (Silverman et al. 2012) at $t \approx \pm 3$ days. However, SN 2013dy resembles the normal SN 2003du and SN 2011fe observationally. The weak Si II absorptions (i.e., $\sim 70.7 \text{ \AA}$ and $\sim 3.3 \text{ \AA}$ for Si II $\lambda 6355$ and $\lambda 5972$, respectively), however, put it into the transitional region of SS and CN at the near-side of the former in the Branch et al. (2006) diagram, as shown in Figures 14(a) and (c). It is difficult to distinguish the SS/91T-like from SS/NL in this scheme. SN 2013dy is also close to the NL SN 2012fr. However, the 91T/99aa-like events keep away from NL SNe Ia in the Wang et al. (2009a) diagram owing to the difference in velocity, as shown in Figures 14(b) and (d). In the Wang et al. (2009a) scheme, SN 2013dy and SN 2012fr are also separated and the former resides at the border between the NV and the 91T/99aa-like subclasses. The slow decline rate, the small EW of Si II absorptions, and the low velocity gradient resemble the properties of the 91T/99aa-like objects. Besides, the $U - B$ color of SN 2013dy is as blue as that of SN 1999aa at the early phase. However, the absence of Fe III lines in the early spectra of SN 2013dy is a clear distinction from 91T/99aa-like events.

6. CONCLUSION

We have presented extended observations of Type Ia SN 2013dy obtained at LJT, XLT, TNT, and *Swift*-UOVT.

Combined with the data published in Z13 and P15, this target is a well-sampled SN Ia with wide wavelength coverage (i.e., from $\sim 1600 \text{ \AA}$ to $\sim 18000 \text{ \AA}$). In general, this SN resembles normal SNe Ia (e.g., SN 2003du and SN 2011fe) in both photometry and spectroscopy. Nevertheless, it also shares some similarities with the 99aa-like events, such as the $U-B$ and “ $uvm2 - uu$ ” color before maximum, the small decline rate, the low velocity gradient, and the small ratios of $R(\text{Si II})$, $R(\text{S/Fe})$, and $R(\text{Si/Fe})$. However, the absence of Fe III lines in the early spectra of SN 2013dy might exclude it from 91T/99aa-like group.

A problem is the uncertainty of the distance. In general, the distance (i.e., $D \approx 20.0 \text{ Mpc}$) derived from several methods seems to be more reasonable than the estimations from the Tully–Fisher relation of the host galaxy (i.e., $D \approx 13.7 \text{ Mpc}$). Based on the larger one, we estimated the peak brightness (e.g., $M_{\text{max}}(B) = -19.65 \pm 0.40 \text{ mag}$), maximum bolometric luminosity ($[1.95 \pm 0.55] \times 10^{43} \text{ erg s}^{-1}$), and synthesized nickel mass ($0.90 \pm 0.26 M_{\odot}$). The distance derived from the Tully–Fisher relation will yield fainter results (i.e., $M_B = -18.83 \pm 0.3 \text{ mag}$; $L_{\text{max}} = [9.05 \pm 2.50] \times 10^{42} \text{ erg s}^{-1}$; $M(^{56}\text{Ni}) = 0.42 \pm 0.15 M_{\odot}$) that are dimmer than the average SNe Ia and do not follow the WLR of SNe Ia well. Additionally, the H band luminosity of SN 2013dy is at least 1.0 mag fainter than the average SNe Ia. That might indicate inefficient emission translation from optical to NIR for SN 2013dy or imply that this SN is an intrinsically fainter SN Ia, although it shows a small $\Delta m_{15}(B)$. Moreover, the H band photometry of SN 2013dy and SN 2011hr suggests a larger scatter (i.e., $\sim 2.0\text{--}2.5 \text{ mag}$) among the SNe Ia with a slow decline rate (e.g., $\Delta m_{15}(B) \approx 0.90 \text{ mag}$) and might challenge the assumption of the uniform NIR luminosity for SNe Ia.

On the other hand, it is difficult to put SN 2013dy into one subclass in the current classification system. The spectroscopy classification reveals that SN 2013dy might be a transitional event residing on the border of different subclasses, such as SS-CN in the Branch et al. (2006) classification scheme or NV-91T/99aa-like in the Wang et al. (2009a) classification system. Moreover, the diversity of the SNe Ia with small $\Delta m_{15}(B)$ and EWs of Si II (e.g., the superluminous SNe Ia, the 91T/99aa-like events, the SN 2012fr-like events, and SN 2013dy) might imply the only EW criterion is insufficient for the classification of this sample and indicate a complex construction of their ejecta.

All of these suggest that SN 2013dy might not be a typical SNe Ia, although it is normal in some respects. Further modeling work is essential to reveal the nature of this SN.

We thank the anonymous referee for constructive suggestions that helped to improve the paper. We acknowledge the support of the staff of the Li-Jiang 2.4 m telescope (LJT), Xin-Long 2.16 m telescope, and Tsinghua-NAOC 0.8 m telescope (TNT). Funding for the LJT has been provided by Chinese academe of science (CAS) and the People’s Government of Yunnan Province. The TNT is owned by Tsinghua University and operated by the National Astronomical Observatory of the Chinese Academy of Sciences (NAOC). The data from UVOT comes from the *Swift* Data Center. We also thank Dr. Wei-Kang Zheng of UC Berkeley who provided the early $BVRI$ photometry of SN 2013dy (Z13).

Financial support for this work has been provided by the National Science Foundation of China (NSFC, grants

11403096, 11178003, 11325313, 11133006, 11361140347, 11203034, 11203078, 11573069, 11303085, 11203070); the Major State Basic Research Development Program (2013CB834903); the Strategic Priority Research Program “The Emergence of Cosmological Structures” of the CAS (grant No. XDB09000000); the Key Research Program of the CAS (Grant NO. KJZD-EW-M06); the CAS “Light of West China” Program; the Youth Innovation Promotion Association of the CAS; the Open Project Program of the Key Laboratory of Optical Astronomy, NAOC, CAS; and the key Laboratory for Research in Galaxies and Cosmology of the CAS.

REFERENCES

- Arnett, W. D. 1982, *ApJ*, 253, 785
- Barone-Nugent, R. L., Lidman, C., Wyithe, J. S. B., et al. 2012, *MNRAS*, 425, 1007
- Benetti, S., Cappellaro, E., Mazzali, P. A., et al. 2005, *ApJ*, 623, 1011
- Bessell, M. S. 1990, *PASP*, 102, 1181
- Blondin, S., Matheson, T., Kirshner, R. P., et al. 2012, *AJ*, 143, 126
- Branch, D., Dang, L. C., & Baron, E. 2009, *PASP*, 121, 238
- Branch, D., Dang, L. C., Hall, N., et al. 2006, *PASP*, 118, 560
- Brown, P. J. 2014, arXiv:1408.1033v1
- Brown, P. J., Breeveld, A. A., Holland, S., et al. 2014, *AP&SS*, 354, 89
- Brown, P. J., Dawson, K. S., & Pasquale, M. 2012, *ApJ*, 753, 22
- Brown, P. J., Roming, P. W., Milne, P., et al. 2010, *ApJ*, 721, 1608
- Cardelli, J. A., Clayton, G. C., & Mathis, J. S. 1989, *ApJ*, 345, 245
- Casper, C., Zheng, W., Li, W., Filippenko, A. V., & Cenko, S. B. 2013, *CBET*, 3588, 1
- Childress, M. J., Hillier, D. J., Seitzzahl, I., et al. 2015, *MNRAS*, 454, 3815
- Childress, M. J., Scalzo, R. A., Sim, S., et al. 2013, *ApJ*, 770, 29
- Chotard, N., Gangler, E., Aldering, G., et al. 2011, *A&A*, 529L, 4C
- Cousins, A. 1981, *SAAOC*, 6, 4
- Fan, Y. F., Bai, J. M., Zhang, J. J., et al. 2015, *RAA*, 15, 918
- Filippenko, A. V. 1992a, *ApJL*, 384, L15
- Filippenko, A. V. 1992b, *AJ*, 104, 1543
- Folatelli, G., Phillips, M. M., Burns, C. R., et al. 2010, *AJ*, 139, 120
- Foley, R. J. 2012, *ApJ*, 748, 127
- Foley, R. J., Sanders, N. E., & Kirshner, R. P. 2011, *ApJ*, 742, 89
- Garavini, G., Folatelli, G., Goobar, A., et al. 2004, *ApJ*, 128, 387
- Gehrels, N., Chincarini, G., Giommi, P., et al. 2004, *ApJ*, 611, 1005
- Hachinger, S., Mazzali, P. A., & Benetti, S. 2006, *MNRAS*, 370, 299
- Howell, D. A., Sullivan, M., Nugent, P. E., et al. 2006, *Natur*, 443, 308
- Huang, F., Li, J. Z., Wang, X. F., et al. 2012, *RAA*, 11, 1585
- Jha, S., Kirshner, R. P., Challis, P., et al. 2006, *AJ*, 131, 527
- Johnson, H., Iriarte, B., Mitchell, R., & Wisniewski, W. 1966, *CoLPL*, 4, 99
- Kattner, S., Leonard, D. C., Burns, C. R., et al. 2012, *PASP*, 124, 114
- Krisciunas, K., Phillips, M. M., & Suntzeff, N. B. 2004, *ApJL*, 602, L81
- Landolt, A. V. 1992, *AJ*, 104, 340
- Li, W., Filippenko, A., Ryan, C., et al. 2003, *PASP*, 115, 453
- Matheson, T., Joyce, R. R., Allen, L. E., et al. 2012, *ApJ*, 754, 19
- Mazzali, P. A., Benetti, S., Altavilla, G., et al. 2005a, *ApJ*, 623L, 37
- Mazzali, P. A., Benetti, S., Stehle, M., et al. 2005b, *MNRAS*, 357, 200
- Mazzali, P. A., Danziger, I. J., & Turatto, M. 1995, *A&A*, 297, 509
- Mazzali, P. A., Röpke, F. K., Benetti, S., & Hillebrandt, W. 2007, *Sci*, 315, 825
- Mazzali, P. A., Sullivan, M., Hachinger, S., et al. 2014, *MNRAS*, 439, 1959
- Meikle, W. P. S. 2000, *MNRAS*, 314, 782
- Mould, J. R., Huchra, J. P., Freedman, W. L., et al. 2000, *ApJ*, 529, 786
- Munari, U., Henden, A., Belligoli, R., et al. 2013, *NewA*, 20, 30
- Nasonova, O. G., de Freitas Pacheco, J. A., & Karachentsev, I. D. 2011, *A&A*, 523, 104
- Nugent, P. E., Baron, E., Branch, D., et al. 1997, *ApJ*, 485, 812
- Nugent, P. E., Sullivan, M., Cenko, S. B., et al. 2011, *Natur*, 480, 344
- Pan, Y.-C., Foley, R. J., Challis, P., et al. 2015, *MNRAS*, 452, 4307 (P15)
- Parrent, J. T., Thomas, R. C., Fesen, R. A., et al. 2011, *ApJ*, 732, 30
- Pereira, R., Thomas, R., Aldering, G., et al. 2013, *A&A*, 554, A27
- Phillips, M. 1993, *ApJL*, 413, L105
- Phillips, M., Lira, R., Suntzeff, N. B., et al. 1999, *AJ*, 118, 1766
- Poole, T., Breeveld, A., Page, M., et al. 2008, *MNRAS*, 383, 627
- Poznanski, D., Ganeshalingam, M., Silverman, J. M., & Filippenko, A. V. 2011, *MNRAS*, 415, L81

- Roming, P., Kennedy, T., Mason, K., et al. 2005, *SSRv*, 120, 95
- Scalzo, R., Aldering, G., Antilogus, P., et al. 2010, *ApJ*, 713, 1073
- Schlafly, E. F., & Finkbeiner, D. P. 2011, *ApJ*, 737, 103
- Schlegel, D., Finkbeiner, D., & Davis, M. 1998, *ApJ*, 500, 525
- Silverman, J., Foley, R. J., Filippenko, A. V., et al. 2012, *MNRAS*, 425, 1789
- Silverman, J., Ganeshalingam, M., Li, W., et al. 2011, *MNRAS*, 410, 585
- Silverman, J. M., & Filippenko, A. V. 2012, *MNRAS*, 425, 1917
- Smitka, M. T., Brown, P. J., Suntzeff, N. B., et al. 2015, *ApJ*, 813, 30
- Stanishev, V., Goobar, A., Benetti, S., et al. 2007, *A&A*, 469, 645
- Stetson, P. 1987, *PASP*, 99, 191
- Stritzinger, M., & Leibundgut, B. 2005, *A&A*, 431, 423
- Stritzinger, M., Mazzali, P. A., Sollerman, J., & Benetti, S. 2006, *A&A*, 460, 793
- Taubenberger, S., Benetti, S., Childress, M., et al. 2010, *MNRAS*, 412, 2735
- Tully, R. B., Rizzi, L., Shaya, E., et al. 2009, *AJ*, 138, 323
- Turatto, M., Benetti, S., & Cappellaro, E. 2003, in *From Twilight to Highlight: The Physics of Supernovae*, ed. W. Hillebrandt, & B. Leibundgut (Berlin: Springer), 200
- Wang, X., Filippenko, A. V., Ganeshalingam, M., et al. 2009a, *ApJL*, 699, L139
- Wang, X., Li, W., Filippenko, A., et al. 2009b, *ApJ*, 697, 380
- Wang, X., Li, W., Filippenko, A. V., et al. 2008, *ApJ*, 675, 626
- Wang, X., Wang, L., Filippenko, A., et al. 2013, *Sci*, 340, 170
- Weyant, A., Michael, W., Allen, L., et al. 2014, *ApJ*, 784, 105
- Zhang, J. J., & Wang, X. F. 2013, *CBET*, 3558, 3
- Zhang, J. J., Wang, X. F., Bai, J. M., et al. 2014, *AJ*, 148, 1
- Zhang, J. J., Wang, X. F., Sasdelli, M., et al. 2016a, *ApJ*, 817, 1154
- Zhang, K. C., Wang, X. F., Zhang, J. J., et al. 2016b, *ApJ*, in press (arXiv:1602.02951)
- Zheng, W. K., Silverman, J. M., Filippenko, A. V., et al. 2013, *ApJL*, 778, L15 (Z13)